JGR Oceans

RESEARCH ARTICLE

10.1029/2024JC021515

Key Points:

- Advection from mean ocean currents reinforces net heat flux warming prior to the MJO initiation in the western Indian Ocean
- MJO induced ocean currents within the Maritime Continent modulate intraseasonal anomalies of mixed layer temperature
- Intraseasonal mixed layer heat budget is dominated by ocean advection at smaller horizontal scales and by the net heat flux at larger scales

Supporting Information:

Supporting Information may be found in the online version of this article.

Correspondence to:

E. Karlowska,
e.karlowska@uea.ac.uk

Citation:

Karlowska, E., Matthews, A. J., Webber, B. G. M., Graham, T., & Xavier, P. (2024). The relative importance of ocean advection and surface heat fluxes during the Madden–Julian Oscillation in a coupled ocean–atmosphere model. *Journal of Geophysical Research: Oceans*, *129*, e2024JC021515. https://doi.org/10.1029/2024JC021515

Received 10 JUL 2024
Accepted 27 OCT 2024

Author Contributions:

Conceptualization: E. Karlowska, A. J. Matthews, B. G. M. Webber, T. Graham, P. Xavier
Data curation: T. Graham, P. Xavier
Formal analysis: E. Karlowska
Funding acquisition: A. J. Matthews, B. G. M. Webber, T. Graham, P. Xavier
Investigation: E. Karlowska
Methodology: E. Karlowska, A. J. Matthews, B. G. M. Webber, T. Graham, P. Xavier
Project administration: A. J. Matthews, B. G. M. Webber, T. Graham, P. Xavier
Resources: A. J. Matthews, B. G. M. Webber, T. Graham, P. Xavier

The Relative Importance of Ocean Advection and Surface Heat Fluxes During the Madden–Julian Oscillation in a Coupled Ocean–Atmosphere Model

E. Karlowska[1,2], A. J. Matthews[3], B. G. M. Webber[1], T. Graham[2], and P. Xavier[2]

[1]Centre for Ocean and Atmospheric Sciences, School of Environmental Sciences, University of East Anglia, Norwich, UK, [2]Met Office, Exeter, UK, [3]Centre for Ocean and Atmospheric Sciences, School of Environmental Sciences and School of Mathematics, University of East Anglia, Norwich, UK

Abstract Intraseasonal variability of ocean surface mixed layer temperature (MLT) in the tropics can be linked to the Madden–Julian Oscillation (MJO), the main source of intraseasonal atmospheric variability in the tropics. Here, we conduct a boreal winter mixed layer heat budget using 10-day forecast composites of a coupled ocean–atmosphere Numerical Weather Prediction model of the UK Met Office to reveal that ocean advection plays a major role in modulating intraseasonal anomalies of MLT over the tropical Indian Ocean and the Maritime Continent. Large scale (∼10°) intraseasonal anomalies of MLT (∼0.1 °C) are driven by net surface heat flux. Ocean advection dominates at smaller horizontal scales (∼1°), contributing up to 0.5 °C to the intraseasonal MLT anomaly. Prior to the development of the enhanced MJO convection in the western Indian Ocean (phases 8 and 1), ocean advection reinforces the net heat flux warming in this region. However, ocean advection opposes the net heat flux warming in the Maritime Continent prior to the development of suppressed MJO convection in this region. When the MJO convection develops over the central Indian Ocean (phase 3), ocean advection (net surface heat flux) drives the intraseasonal MLT anomalies in the western Indian Ocean (central Indian Ocean and the Maritime Continent). Our results demonstrate the importance of ocean dynamics during the initiation and growth of the MJO, and raise implications for models that do not resolve these processes.

Plain Language Summary The Madden–Julian Oscillation (MJO) is a large-scale tropical convection pattern, originating in the western Indian Ocean and traveling eastward across the tropics. The MJO lasts 1–3 months and is often linked to extreme weather across the globe. Oceanic processes can modulate the MJO through the exchange of momentum, moisture and heat between the ocean and the atmosphere. Here, we analyze 10 days forecasts using a coupled ocean–atmosphere model to find the role of the oceanic currents in the modulation of the MJO related ocean temperature changes in the upper 10–100 m of the ocean. Prior to the development of the MJO convection in the western Indian Ocean, the movement of warm and cold water by the ocean currents and the surface net heat flux (warming or cooling of the ocean surface due to changes in solar radiation and evaporation) dominate the MJO-related upper ocean temperature changes in the western Indian Ocean. When the MJO reaches the central Indian Ocean, the surface net heat flux dominates in the central Indian Ocean and western Pacific. Our results demonstrate that ocean dynamics are important on MJO timescales and should be adequately represented in weather and climate models.

1. Introduction

The ocean surface mixed layer is a layer of approximately constant temperature and salinity, typically from the surface to between 10 and 100 m depth in the tropics (de Boyer Montégut et al., 2004). The depth of the ocean surface mixed layer varies due to changes in incoming solar radiation and heat fluxes at the ocean surface, wind-driven mechanical mixing, and the influx of freshwater into the ocean. Intraseasonal variations of the mixed layer temperature (MLT; closely related to sea surface temperature) in the tropics can be linked to the evolution of the Madden–Julian Oscillation (MJO) (Chi et al., 2014; Drushka et al., 2012; Halkides et al., 2015; McPhaden & Foltz, 2013), the dominant mode of intraseasonal (30–90 days) atmospheric variability in the tropics. The canonical MJO event is comprised of large-scale (∼ 10,000 km) enhanced and suppressed convective anomalies traveling eastward in the tropics at ∼5 m s^{-1} phase speed (Madden & Julian, 1971, 1972). The MJO originates in the western Indian Ocean and travels through the Maritime Continent (MC; Indonesia, Philippines and Papua New Guinea), until it dissipates over the western Pacific.

Software: E. Karlowska, A. J. Matthews
Supervision: A. J. Matthews, B. G. M. Webber, T. Graham, P. Xavier
Validation: E. Karlowska
Visualization: E. Karlowska
Writing – original draft: E. Karlowska
Writing – review & editing: E. Karlowska, A. J. Matthews, B. G. M. Webber, T. Graham, P. Xavier

The suppressed phase of the MJO is characterized by calm, cloud free, and sunny conditions, leading to a reduction in mechanical mixing in the surface ocean, shoaling of the mixed layer, and enhancement of sea surface temperatures (SSTs). Warm SSTs promote evaporation into the atmosphere and lead to instability and atmospheric convection. Observations show that warm intraseasonal SST anomalies occur 1 week prior to the MJO convection over the Indo-Pacific warm pool region (Hendon & Glick, 1997; Woolnough et al., 2000). The development of the convective MJO anomalies is associated with an increase in cloud cover and surface winds, leading to a decrease in solar radiation at the ocean surface and an increase in mechanical mixing. This, in turn, leads to the deepening of the mixed layer and cooling of the SST (Drushka et al., 2012; Liu et al., 2021). Thus, the MJO suppressed phase promotes warm intraseasonal SST anomalies and the MJO convective phase contributes to the cooling of intraseasonal SST anomalies in the Indo-Pacific warm pool (Itterly et al., 2021; Yan et al., 2021). As a result, a coupled feedback mechanism exists whereby convective and SST anomalies both propagate eastwards, out of phase by a quarter of a cycle, with anomalies in the atmosphere and ocean reinforcing each other.

The role of ocean dynamics in the initiation and sustenance of the MJO is still debated in the scientific community (e.g., DeMott et al., 2015; Sobel et al., 2010; Zhang, 2005). The MJO is predominantly an atmospheric phenomenon, and atmosphere-only models are able to successfully reproduce an eastward propagating MJO without a dynamically evolving ocean (e.g., Karlowska et al., 2024a; Woolnough et al., 2007). However, air–sea interactions are known to play an important role during the MJO (DeMott et al., 2015; Y. Li et al., 2013). Mixed layer heat budgets are conducted to investigate the relative importance of oceanic subsurface processes and heat flux forcing on the intraseasonal changes of the MLT during the MJO (Chi et al., 2014; Drushka et al., 2012; Halkides et al., 2015; McPhaden & Foltz, 2013). Drushka et al. (2012) conducted a mixed layer heat budget using in situ observations of Argo floats in the Indo-Pacific warm pool region and showed that the net heat flux changes associated with the eastward propagating MJO convective envelope are the main driver of the intraseasonal MLT changes. Their budget, however, did not close. The analyses of moorings by Chi et al. (2014) and McPhaden and Foltz (2013) showed that the horizontal advection and the formation of barrier layers can have a substantial effect on the MLT changes during the MJO. The discrepancies in the relative importance of different mixed layer heat budget terms between the studies of Chi et al. (2014) and McPhaden and Foltz (2013), and Drushka et al. (2012) are likely due to shorter data span available from moorings compared with the Argo float data set, and a choice of particular locations for moorings that may not be representative of the wider Indian Ocean basin.

In situ mixed layer heat budgets suffer from certain limitations, therefore, model studies are used to ensure long data span, wide spatial range, and closure of the heat budgets. Halkides et al. (2015) analyzed 18 years of a heat-conserving ocean state estimate to reveal that wind-driven horizontal advection is the largest contributor to the intraseasonal MLT variability near the equator. Away from the equator, they found that vertical subsurface processes (vertical mixing and vertical advection) and net heat fluxes dominate the mixed layer heat budget on MJO timescales (hereafter referred to as the "MJO mixed layer heat budget"). Their study, however, was limited by the lack of eddy activity in their ocean state estimate. Chandra et al. (2024) used an updated version of this data set at a higher temporal frequency that included a parameterization scheme for eddy transport to state that horizontal advection is the main driver of intraseasonal ocean heat content anomalies in the upper 200 m of the tropical Indian Ocean. They argued that the surface heat fluxes play a minor role in the upper ocean heat content variability during the MJO, with a caveat that their study included both the mixed layer and the thermocline. They showed that positive intraseasonal anomalies of the ocean heat content over the Indian Ocean prior to the MJO convection over the MC are partially driven by equatorial oceanic Rossby waves. These waves are generated by equatorial oceanic Kelvin waves that are reflected off the coast of Sumatra and travel westward toward the African coast and bring warm SSTs to the western Indian Ocean basin. This is consistent with previous studies that showed that oceanic Rossby waves contribute to the intraseasonal changes in the upper ocean heat content (Rydbeck et al., 2019, 2023). Rossby waves have also been hypothesized to trigger primary MJO events in the tropics (Webber, Matthews, et al., 2012).

In this paper, a mixed layer heat budget is conducted in the context of the MJO using a global coupled ocean–atmosphere Numerical Weather Prediction (NWP) model of the UK Met Office. An eddy-permitting coupled model is used to address the relative importance of ocean advection and the net heat flux forcing in modulating the MJO-related mixed layer temperature changes in the tropical Indian Ocean and the MC. In Section 2, model specifications, data, and methodology are described. In Section 3, the mixed layer heat budget is conducted targeting three different MJO phases (pre-initiation, initiation, and maturity), and a novel approach is presented to

Table 1
Model Specifications Summary

Start date	End date	Atmosphere horizontal resolution	Atmosphere no. of levels	Ocean horizontal resolution	Ocean no. of levels	Global atmosphere (GA) version	Global land (GL) version	Global ocean (GO) version	Global sea ice (GSI) version
1 May 2016	24 Sep 2018	N216	L85	ORCA025	L75	GA6.1	GL6.1	GO5	GSI6
25 Sep 2018	31 May 2021	N320	L70	eORCA025	L75	GA7.2	GL8.1	GO6.0	GSI8.0

Note. References: GA6.1 and GL6.1 (Walters et al., 2017); GA7.2, GA7.2.1, and GL8.1 (Walters et al., 2019); GO5 (Megann et al., 2014); GO6.0 (Storkey et al., 2018); GSI6 (Rae et al., 2015); GSI8.0 and GSI8.1 (Ridley et al., 2018).

separate different horizontal scales at which oceanic processes contribute to the changes in the intraseasonal MLT. Discussion and conclusions follow in Section 4.

2. Data and Methods

2.1. Model Specifications

The data used in this study were generated with the coupled ocean–atmosphere NWP system of the UK Met Office. The model was run in a hindcast mode for a 5 year period between 1 May 2016 and 31 May 2021, and initialized at 0000 UTC each day, yielding 1857 forecasts. Each model run was integrated out to 15 forecast days. The model used in this study is a version of the operational Met Office model running at the time, hence, some of the operational changes were applied to this model on 24 September 2018 (see Table 1 for detailed model versions and their references). The horizontal resolution of the atmosphere component was N216 from 1 May 2016 to 24 September 2018 (0.83° longitude and 0.56° latitude). Afterward, the horizontal resolution of the atmosphere component was N320 (0.57° longitude and 0.38° latitude). The atmosphere component of the coupled model uses a convective parameterization scheme, with separate representations of shallow, mid-level, and deep convection (Gregory & Allen, 1991; Gregory & Rowntree, 1990).

The ocean component of the coupled model is the Nucleus for European Modeling of the Ocean (NEMO) consortium ocean model (Madec et al., 2017). The NEMO ocean model is comprised of 75 vertical levels, with 8 model levels in the top 10 m of the ocean. The horizontal resolution of the NEMO ocean model is 0.25°. The NEMO ocean model uses a turbulent kinetic energy scheme for the parameterization of the vertical and horizontal mixing in the ocean model (Madec et al., 2017). The model exchanges information between the ocean–sea ice and the atmosphere–land components with a 1 hr coupling frequency. The ocean–sea ice and atmosphere–land components are initialized separately, with their own data assimilation (DA) systems. The NEMO ocean model uses the Forecast Ocean Assimilating Model (FOAM)-NEMOVAR DA system from Blockley et al. (2014) and Waters et al. (2015) to initialize its SST and sea ice concentrations. The atmosphere–land component is initialized with the 4D-Var DA system (Rawlins et al., 2007) that uses SST and sea ice concentrations from the Operational Sea Surface Temperature and Ice Analysis (OSTIA) (Donlon et al., 2012) assimilation system, updated by E. K. Fiedler et al. (2019) and Good et al. (2020). More detailed model descriptions are available in Section 2 of Vellinga et al. (2020).

2.2. Real-Time Multivariate MJO Index

The Wheeler and Hendon (2004) Real-time Multivariate MJO (RMM) index is used in this study to define the state of the MJO in the tropics. The index is constructed with daily anomalies of top-of-atmosphere outgoing longwave radiation (OLR) and zonal winds at 850 hPa and 200 hPa (full methodology available in Gottschalck et al. (2010), with references therein). The indices RMM1 and RMM2 split the tropics into 8 phases: phases 8 and 1 when the MJO convection is located over Africa and the western hemisphere; phases 2 and 3 when the MJO convection is located over the Indian Ocean; phases 4 to 5 when the MJO travels across the Maritime Continent and phases 6 and 7 when the MJO convection is located over the western Pacific. Observed indices are used in this study, retrieved from http://www.bom.gov.au/climate/mjo (Wheeler & Hendon, 2004). Days with an active MJO are defined for those with RMM amplitude: $\sqrt{\mathrm{RMM1}^2 + \mathrm{RMM2}^2} \geq 1.0$. For a detailed MJO performance analysis in this coupled model, see Karlowska et al. (2024b).

2.3. Mixed Layer Depth, Barrier Layer Thickness, and Thermocline Depth Diagnostics

Mixed layer heat budgets were conducted for selected regions in the tropics in the context of the MJO. Subsurface ocean data were processed to study the evolution of ocean variables in the mixed layer in the coupled model of the UK Met Office. The mixed layer depth was defined following Drushka et al. (2014) as the depth where the potential density (σ) change from the potential density at a reference depth of 10 m is greater than a threshold given by:

$$\Delta\sigma = \sigma(T_{ref} - \Delta T, S_{ref}, P_0) - \sigma(T_{ref}, S_{ref}, P_0), \quad (1)$$

where T_{ref} and S_{ref} are the temperature and salinity at the reference depth 10 m, P_0 is surface pressure. ΔT values of 0.25 °C, 0.5 °C and 0.8 °C were explored and 0.5 °C was chosen as the optimal value for ΔT (not shown). The reference depth of 10 m was chosen to remove the effects of the diurnal cycle of temperature on mixed layer depth (de Boyer Montégut et al., 2007; Hosoda et al., 2010). Temperature and salinity were interpolated in depth to 1 m resolution between 0 and 200 m before calculating the mixed layer depth. Potential density calculations were obtained using Python package gsw v3.4.0 based on definitions from Gibbs SeaWater Oceanographic Toolbox of TEOS-10 (McDougall & Barker, 2011). The barrier layer thickness was calculated as the difference between the isothermal layer depth, defined by the depth where the temperature equals $T_{ref} - \Delta T$, and the mixed layer depth. The thermocline in the tropics typically lies between 15 °C and 25 °C isotherms (e.g., Meyers, 1979; P. C. Fiedler, 2010). The 20 °C isotherm, that is, the mid-point between these isotherms, is generally considered a good proxy for the thermocline depth in the tropics. The 20 °C isotherm depth (D20) was extracted from the model data by a linear interpolation between model levels.

2.4. Composites

Vertical profiles of ocean temperature, temperature tendencies, and ocean currents were vertically averaged within the mixed layer, and weighted by the layer thickness, before further processing. Composite maps were calculated for daily means of mixed layer averages of subsurface ocean variables using the ocean model grid at 0.25° in each region. Separate forecast initializations were concatenated at a given lead time for further processing. Anomalies of all variables are calculated by the removal of the seasonal cycle (annual mean and first three harmonics) for the period 2017–2020. The MJO anomalies are then obtained by a temporal filtering of the anomalies with a 20–200 days bandpass Lanczos filter (Duchon, 1979). Although the MJO produces spectral peaks between 30 and 90 days, this wide bandpass filter is used to avoid spurious maxima and minima before and after an MJO event that are introduced by narrower filter bands such as 30–70 days (Matthews, 2000).

Mean state composites of the MLT $(\overline{T})$ and the mixed layer averaged ocean currents $(\overline{\mathbf{u}})$ were calculated for the boreal winter period from 1 November 2016 to 15 January 2021 for active MJO days. Apart from the mean state composites, every variable in this study refers to an MJO anomaly. Missing forecast initializations (less than 1%) were interpolated between the nearest previous and next day forecast initializations. The statistical significance of the composite MJO anomalies of the mixed layer averaged ocean currents and the mixed layer averaged temperature at the 95% significance level were calculated using a Student's *t*-test.

2.5. Target MJO Phase

Composites for each MJO phase were defined using a "target" MJO phase. The target MJO phase was set to be at T + 10 days within any given forecast run, such that the evolution of the ocean processes that generate the SSTs prior to the target MJO phase can be studied in this coupled model. This timescale was chosen as the typical timescale of the coupling between the MJO convection and the intraseasonal SST anomalies in the tropics (Woolnough et al., 2000). For example, for target MJO phase 3, an initial list of all the days that fall into MJO phase 3 from the RMM indices was first created. A second list was created by subtracting 10 days from all the days in the first list. The composite for the target MJO phase 3 was then calculated using all the forecasts initialized on the days in the second list. Consecutive forecast initializations with the same target MJO phase at T + 10 days were averaged before compositing and treated as one event. Only active MJO forecasts at T + 10 days during the November–April season are used for the composite analysis.

2.6. Mixed Layer Temperature Tendencies

The model provides temperature tendencies due to different oceanic processes: ocean advection (zonal, meridional and vertical), ocean mixing (horizontal and vertical), penetrating solar flux and non-solar fluxes (longwave radiation, latent and sensible heat fluxes), all calculated at the model time step. The following equation describes the temperature tendency in the model:

$$\frac{\partial T}{\partial t} = \underbrace{\left.\frac{\partial T}{\partial t}\right|_{\text{zonal adv.}} + \left.\frac{\partial T}{\partial t}\right|_{\text{merid. adv.}} + \left.\frac{\partial T}{\partial t}\right|_{\text{vert. adv.}}}_{\text{total advection}} + \\ + \left.\frac{\partial T}{\partial t}\right|_{\text{vert. mix.}} + \left.\frac{\partial T}{\partial t}\right|_{\text{horiz. mix.}} + \underbrace{\left.\frac{\partial T}{\partial t}\right|_{\text{solar flux}} + \left.\frac{\partial T}{\partial t}\right|_{\text{non-solar flux}}}_{Q_{net}}, \quad (2)$$

where T is the ocean temperature, t is time, and Q_{net} is the net heat flux. The temperature tendencies due to ocean advection are calculated in the model as the divergence of the advective fluxes. The total temperature tendency due to ocean advection is a sum of the temperature tendencies due to zonal, meridional, and vertical advection. Vertical mixing is parameterized in the model using a turbulent kinetic energy scheme that provides vertical eddy viscosity and diffusivity coefficients through time evolution of the turbulent kinetic energy (Madec et al., 1997, 2017). Horizontal mixing is parameterized in a similar manner to vertical mixing, with the horizontal mixing coefficient varying in 2D space based on the mesh grid size in the model. The temperature tendency due to penetrating solar flux is calculated in the model using the Paulson and Simpson (1977) expression for the attenuation of solar radiation that assumes a constant chlorophyll concentration of 0.05 mg m^{-3} and exponential decay of downward irradiance with depth. The model splits the attenuation of solar radiation into three color bands for wavelengths 400–700 nm (red, green and blue), and one band for wavelengths longer than 700 nm. The model assumes an e-folding depth of 23 m for wavelengths 400–700 nm, and 0.35 m depth for wavelengths longer than 700 nm. The non-solar flux (comprised of longwave radiation, latent and sensible heat fluxes, Q_{nsr}) is distributed in the model within the top model level only. The temperature tendency due to Q_{nsr} is equal to $\frac{Q_{nsr}}{\rho_0 C_p h}$, where $\rho = 1{,}026$ kg m^{-3}, $C_p = 4{,}000$ J/kg°C and $h = 1.02$ m. The horizontal mixing and residual temperature tendencies are not presented in this paper as they are negligible; a typical contribution from the horizontal mixing and the residual to the MJO anomaly of MLT over 10 days of the forecast is 0.0001 °C, three orders of magnitude smaller than the changes in MLT (order 0.1 °C).

MLT tendencies in the model are stored as daily accumulations and all composites of the change in the MJO anomaly of MLT (ΔT) in this paper are summed from forecast day 1–10 to understand the changes in the MLT prior to the arrival of a specific MJO phase in the forecast at T + 10 days. The composites of MLT and ocean currents correspond to daily means centered at 1200 UTC; therefore, all composites of the MLT and the ocean currents (u) in this study correspond to an average between forecast day 1 and 10.

2.7. Observations

Observed values of the daily interpolated OLR were obtained from the National Oceanic and Atmospheric Administration (Liebmann & Smith, 1996).

3. Results

In the following section, three target MJO phases (8, 1, and 3) were chosen to evaluate different oceanic processes contributing to the MJO anomaly of mixed layer temperature (MLT) prior to the arrival of each of these MJO phases at T + 10 days. These phases were chosen to represent the pre-initiation, the initiation, and the maturity of the MJO enhanced convective anomalies over the Indian Ocean. Three regions were chosen for the mixed layer heat budget in the context of the MJO: the western Indian Ocean region (37–60 °E, 10 °S-10 °N), the central Indian Ocean region (65–85 °E, 10 °S-5 °N), and the eastern MC region (120–150 °E, 10 °S-10 °N). The extent of each region is shown in Figure 1c. These regions were chosen as they display the largest changes over the equatorial belt in the MJO anomalies of SST prior to the initiation of the MJO convection over the western Indian Ocean (i.e., phases 8 and 1; Figures 1a–1d).

10.1029/2024JC021515

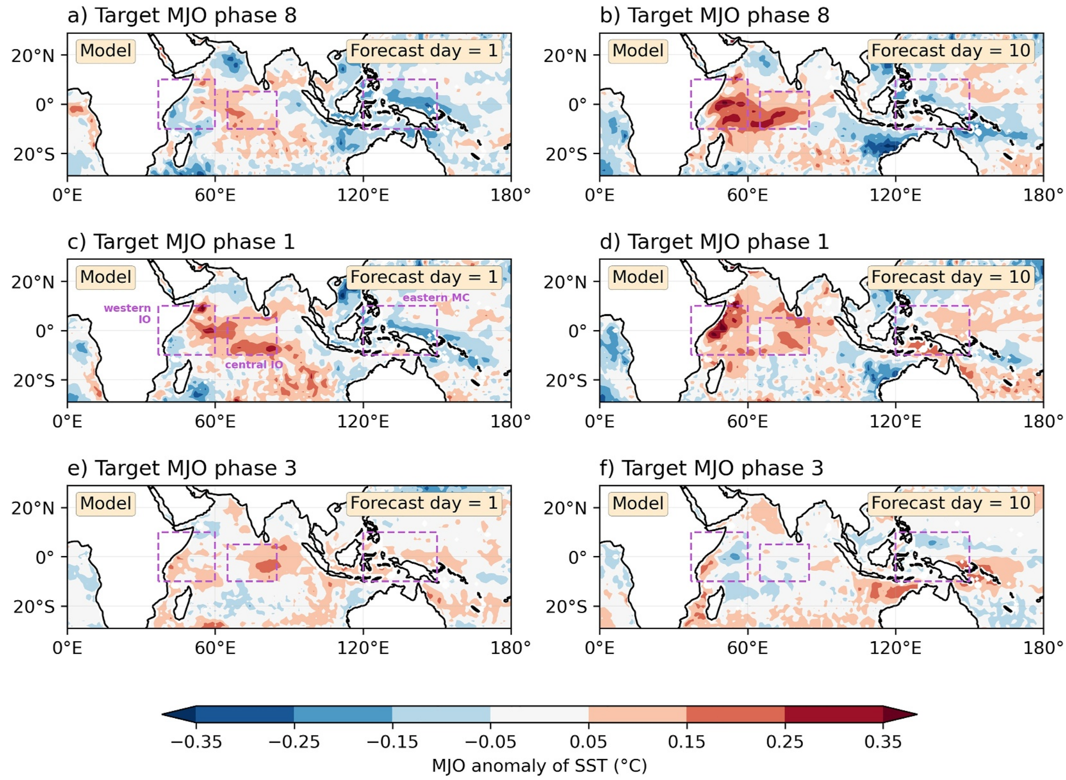

Figure 1. Composite maps of the 20-to-200 days bandpass filtered anomalies (the Madden–Julian Oscillation, MJO anomalies) of model sea surface temperature (SST) for target MJO phases 8 (panels a–b), 1 (panels c–d), and 3 (panels e–f). Panels a, c, and e show composites at forecast day 1 (prior to each MJO phase arrival) and panels (b, d, and f) correspond to forecast day 10 (when each MJO phase arrives in the observations).

3.1. MJO Phase 8: Pre-Initiation

MJO phase 8 represents the pre-initiation stage of the MJO enhanced convective anomalies in the western Indian Ocean region. Observations show that 40% of the primary MJO events initiate in the Indian Ocean, and such events are preceded by warm SST anomalies in that area (Matthews, 2008). In this section, a detailed analysis of the processes driving the warming tendency in SST prior to MJO phase 8 is presented to understand what leads to the development of the subsequent MJO enhanced convective anomalies.

Ten days prior to MJO phase 8 (at forecast day 1), the coupled model simulates a positive MJO anomaly of OLR over the Indian Ocean (suppressed MJO convection) and a negative MJO anomaly of OLR over the western Pacific (enhanced MJO convection) (Figure 2a). The suppressed MJO convection travels eastward into the MC when the MJO is in phase 8 at forecast day 10 (Figure 2b). Additionally, by forecast day 10, a weak enhanced MJO convection develops over the western Indian Ocean. The evolution of the MJO convection prior to MJO phase 8 in the coupled model is consistent with the observed pattern (Figures 2g and 2h), albeit with a stronger suppressed MJO convection over the MC at forecast day 10 in the model compared with observations (Figures 2b and 2h).

The MJO anomalies of SST prior to the MJO phase 8 are warm (cold) over the Indian Ocean (the MC) at forecast day 1 (Figure 1a). Warm MJO anomalies of SST in the western and central Indian Ocean intensify by forecast day 10 when the MJO phase 8 arrives (Figure 1b). These anomalies, of over 0.4 °C, are likely to increase the low level moisture via evaporation and destabilize the atmosphere, which will ultimately lead to more MJO convection in this region later in the forecast and thus support the initiation of the MJO enhanced convective anomalies in phases 8 and 1.

The cumulative change in the MJO anomaly of MLT prior to the MJO phase 8 is positive over the western Indian Ocean region, with up to 0.5 °C increase in the MJO anomaly of MLT ahead of MJO phase 8 (Figure 3a). Total

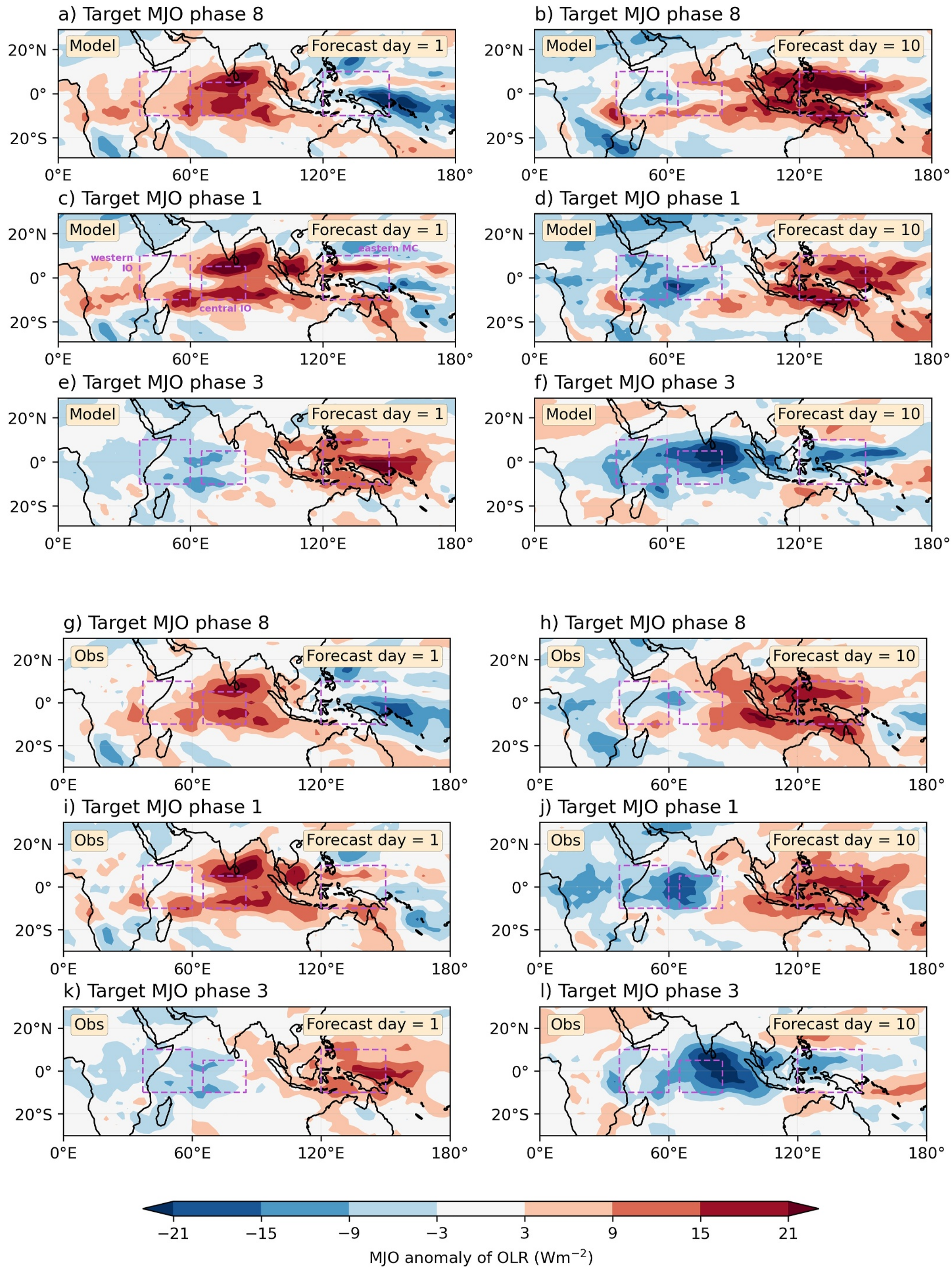

Figure 2. Composite maps of model MJO anomalies of outgoing longwave radiation (OLR) for target MJO phases 8 (panels a–b), 1 (panels c–d), and 3 (panels e–f). Lagged composites of the MJO anomalies of OLR in observations (Liebmann & Smith, 1996) for target MJO phases 8 (panels g–h), 1 (panels i–k) and 3 (panels k–l). Panels (a, c, e, g, i, and k) show composites at forecast day 1 (prior to each MJO phase arrival) and panels (b, d, f, h, j, and l) at forecast day 10 (when each MJO phase arrives in the observations).

advection, vertical mixing, and Q_{net} all contribute to this warming (Figures 3d, 3g, and 3j). The Q_{net} contributes the large scale warming pattern (Figure 3j), whereas the ocean advection and vertical mixing contribute at smaller horizontal scales (Figures 3d and 3g). The warming due to the Q_{net} prior to the MJO phase 8 in this region is consistent with the shoaling of the mixed layer (Figure 4d), which will in turn enhance the magnitude of the heat

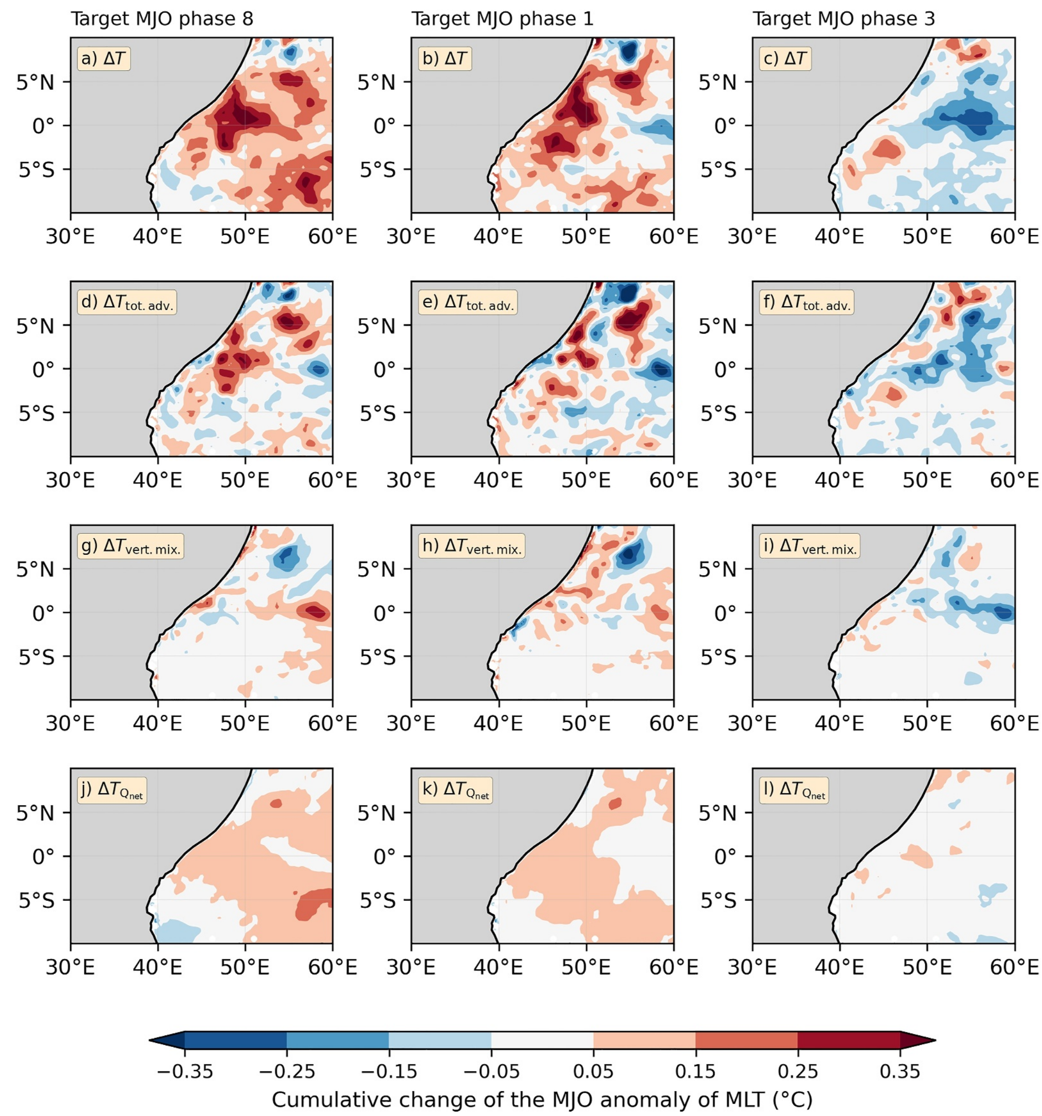

Figure 3. (a–c) Cumulative change in the composite MJO anomaly of mixed layer temperature (MLT) over forecast days 1–10 prior to the arrival of (target) MJO phases 8, 1, and 3 in the western Indian Ocean region; (d–f) cumulative change of the MJO anomaly of MLT due to total advection for target MJO phases 8, 1, and 3; (g–i) cumulative change of the MJO anomaly of MLT due to vertical mixing for target MJO phases 8, 1, and 3; (g–i) cumulative change of the MJO anomaly of MLT due to net heat flux for target MJO phases 8, 1, and 3.

flux driven warming. The total ocean advection reinforces the Q_{net} in this region, contributing up to 0.4 °C to the MJO anomaly of MLT (Figure 3d). Suppressed vertical mixing leads to a 0.25 °C warming near the equator at 55 °E (Figure 3g). However, this warming tendency is canceled by the cooling associated with the total advection at this location (Figure 3d).

Ocean advection prior to MJO phase 8 in the western Indian Ocean is the strongest at the equator near the coast of Africa (Figure 3d). The horizontal advection (zonal and meridional) dominates the total advection term (Figure 5a), consistent with Halkides et al. (2015). The average MJO anomaly of MLT in this region prior to MJO phase 8 is positive to the east of 45 °E and negative near the coast (Figure 5g). The mean ocean currents in the coupled model are westward at the equator and south-westward along the coast of Africa between 5°S and 5°N (Figure 5d). These currents will advect this warm MJO anomaly of MLT westward toward the coast of Africa prior to the MJO convection initiation in this region. Advection of the MJO MLT anomalies by the mean currents appears to be the leading cause of the anomalous warming due to horizontal advection, thus implying that this

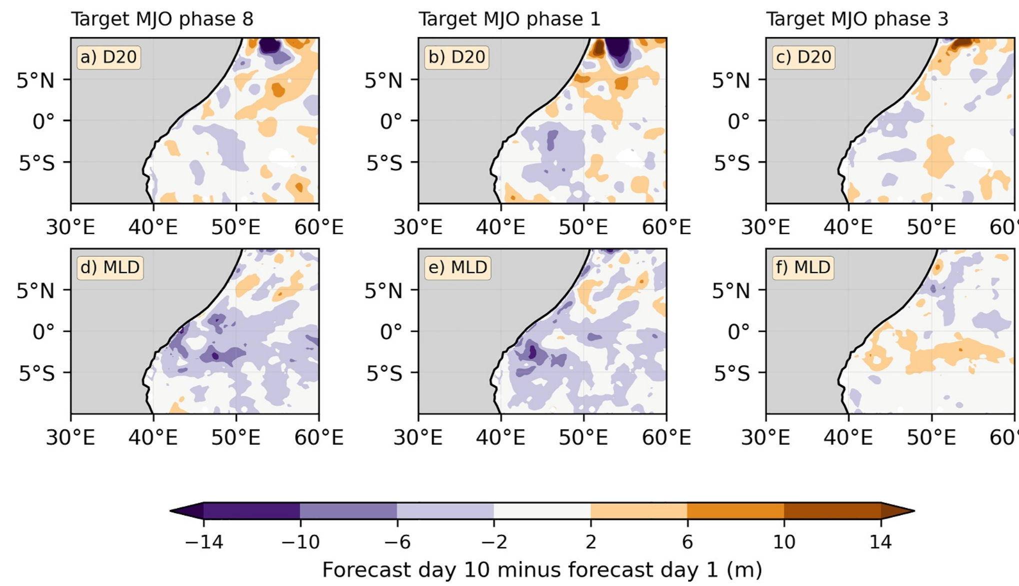

Figure 4. Change in the MJO anomaly of 20° isotherm depth (D20, panels (a–c) and the mixed layer depth (MLD, panels d–f) from forecast day 1–10 prior to the arrival of (target) MJO phases 8, 1, and 3. Target MJO phase 8 in panels (a, d), target MJO phase 1 in panels (b, e), and target MJO phase 3 in panels (c, f).

process is key in generating the warm SST anomalies that precede the initiation of convection here in MJO phases 8 and 1.

Deepening of the D20 and warm MLT tendency ahead of the MJO initiation can be associated with a downwelling oceanic equatorial Rossby wave (Webber, Stevens, et al., 2012). Such waves have a period of ~100 days, and they can produce a signal in the MJO anomalous ocean currents. There are statistically significant westward MJO anomalies of ocean currents at 45–50 °E (Figure 5g). However, the MJO winds are weak prior to the MJO phase 8 in this area (not shown). There are also no notable changes in the MJO anomaly of D20 over 10 forecast days prior to the arrival of the MJO phase 8 (Figure 4a). Therefore, there is little evidence that MJO induced equatorial oceanic waves contribute substantially to the advection-driven warming in these composites.

Over the central Indian Ocean region, the MJO anomaly of MLT shows a warming tendency prior to MJO phase 8 (Figure 6a). This warming is mostly driven by Q_{net} (Figure 6j). The total advection term is noisy in this region (Figure 6d). The most coherent signal is the negative change in the MJO anomaly of MLT of up to 0.25 °C at the equator near 65 °E. This is likely caused by the advection of colder MJO anomalies of MLT toward the east from 70 °E by the mean state ocean currents (not shown). The MJO anomalies of D20 and the mixed layer depth display shoaling in the central Indian Ocean region by up to 6 m prior to the MJO phase 8 (panels a, d in Figure S8 in Supporting Information S1). The mixed layer in this region is at an average depth of 33 m, and a change of 20% in the mixed layer depth is significant. The shoaling of the mixed layer will enhance the warming due to the Q_{net} in this region. The vertical mixing contribution to the MJO anomaly of MLT in this region is negligible prior to MJO phase 8 (Figure 6g).

The eastern MC experiences a cooling of up to −0.25 °C in the MJO anomaly of MLT prior to MJO phase 8 across most of the region (Figure 7a). The total advection is the main driver of this cold MJO anomaly of MLT (up to −0.15 °C, Figure 7d). There is also a negative contribution from the vertical mixing anomalies in this area of up to −0.7 °C (Figure 7g), and a positive contribution from the Q_{net} of up to 0.15 °C (Figure 7j).

The horizontal advection is the main contributor to the total advection term in the eastern MC region prior to the MJO phase 8 arrival (Figure 8a). To further understand the horizontal advection term in this region, Reynolds decomposition is applied to the mean state variables and the MJO anomalies of ocean variables as follows:

$$\Delta T_{\text{horiz. adv.}} = \overline{\mathbf{u}}.\nabla T' + \mathbf{u}'.\nabla \overline{T} + \mathbf{u}'.\nabla T' + \text{residual} \quad (3)$$

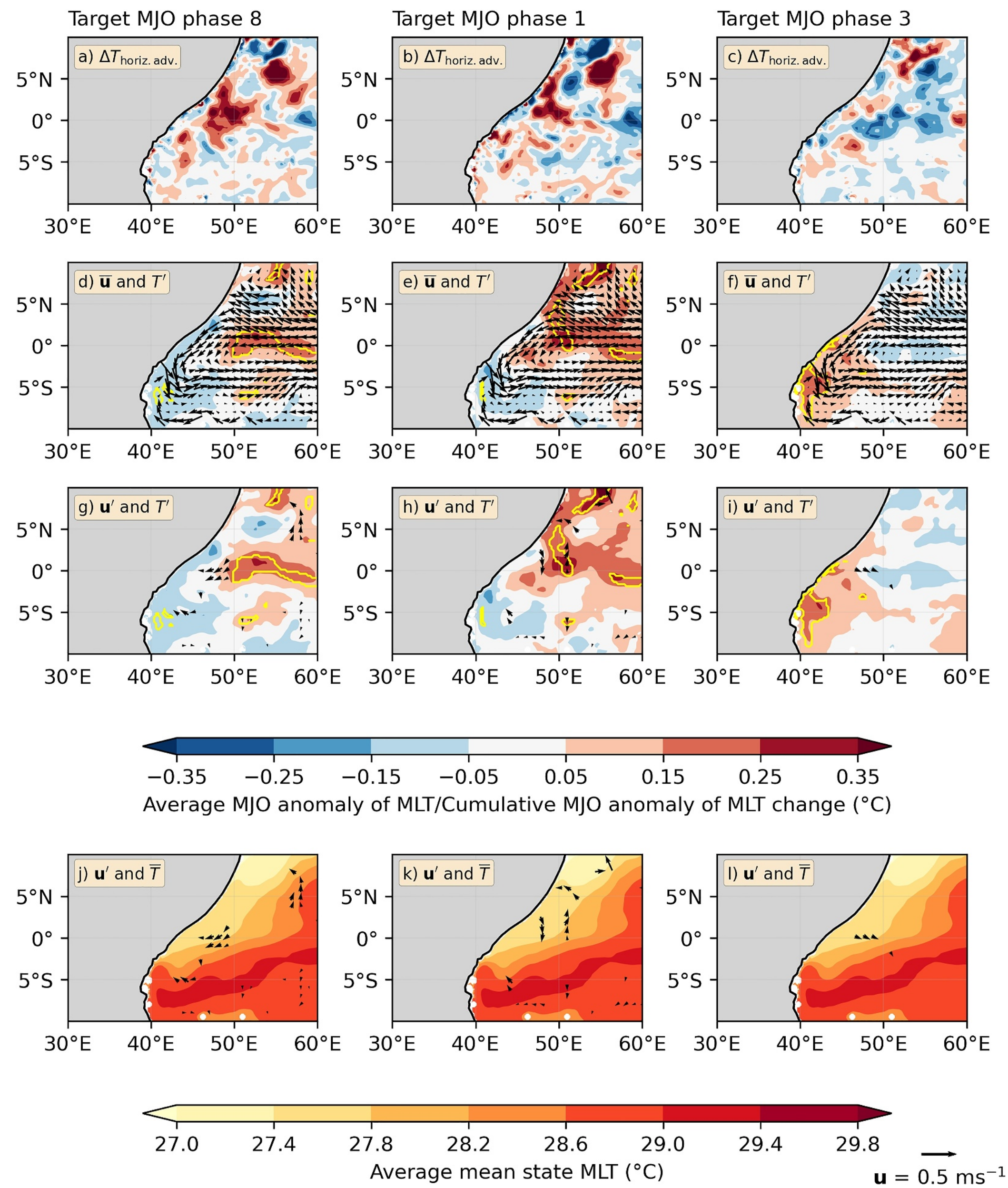

Figure 5. (a–c) Cumulative change in the composite MJO anomaly of mixed layer temperature (MLT) over forecast days 1–10 prior to the arrival of (target) MJO phases 8, 1, and 3 in the western Indian Ocean region due to the horizontal advection; (d–f) average mean state ocean currents in the mixed layer $(\overline{\mathbf{u}})$ and the average MJO anomaly of MLT (T') over forecast days 1–10 in target MJO phases 8, 1, and 3; (g–h) MJO anomalous ocean currents $(\mathbf{u}')$ in the mixed layer $(\overline{\mathbf{u}})$ and T' over forecast days 1–10 in target MJO phases 8, 1, and 3; (j–l) $\mathbf{u}'$ and $\overline{T}$. $\mathbf{u}'$ is plotted at the 95% significance level. Yellow outline shows T' at 95% significance level.

where prime denotes the MJO anomalies of oceanic variables and bar denotes the mean state values (for boreal winter and active MJO). Note that the $\overline{\mathbf{u}}.\nabla\overline{T}$ term is omitted from the equation because it does not affect anomalies. The horizontal advection term in the eastern MC region is reproduced well with Reynolds decomposition in each target MJO phase (Figures 8a and 8m; Figures 8b and 8n; Figures 8c and 8o).

Earlier, we showed that the mean state currents advect the MJO anomalies of MLT in the Indian Ocean to modulate the total MLT tendency in the context of the MJO prior to the MJO phase 8. In contrast, in the eastern MC, the MJO induced ocean current anomalies advecting the mean temperature gradients $(\mathbf{u}'.\nabla\overline{T})$ are the main

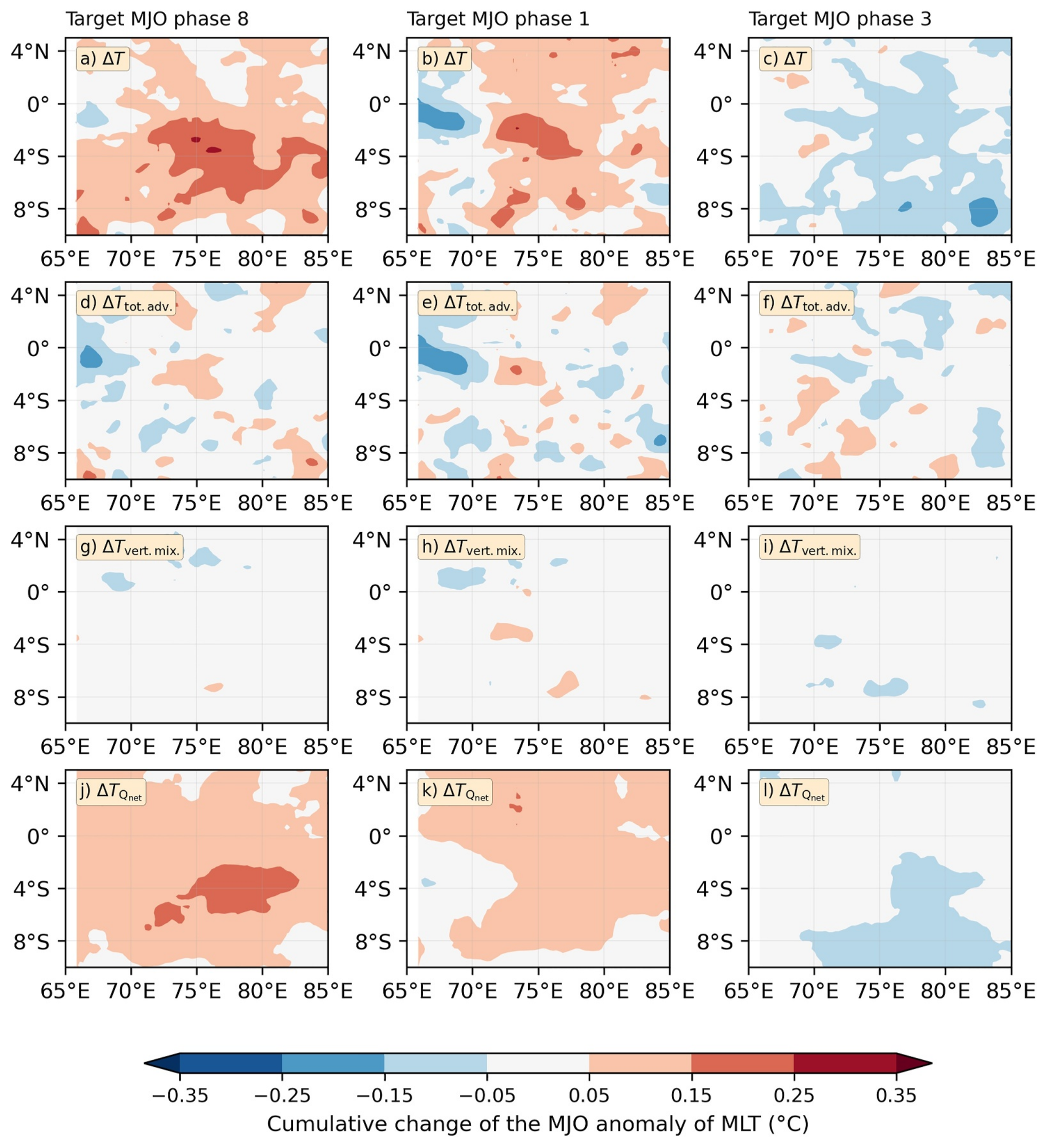

Figure 6. As Figure 3 but for central Indian Ocean region.

driver of the cooling due to the advection in this region prior to the MJO phase 8 (Figure 8g). The other terms, $\bar{\mathbf{u}}.\nabla T'$ and $\mathbf{u}'.\nabla T'$, do not produce a spatially coherent pattern of cooling in this region prior to the MJO phase 8 (Figures 8d and 8j).

The mean state ocean currents off the coast of New Guinea show the South Equatorial Current that travels northwest from New Guinea toward the Banda Sea and the Philippines (Figure 9d). The anti-cyclonic curvature present in the mean state ocean currents near 130–140 °E is likely associated with the semi-permanent and anti-cyclonic Halmahera eddy that the coupled model starts to resolve. The MJO-induced mixed layer ocean current anomalies prior to MJO phase 8 oppose the South Equatorial Current here, reducing the advection of warm water from New Guinea toward Mindanao, thus contributing to the net cooling in this region (Figure 9j). These ocean current anomalies are consistent with the MJO anomalous surface winds in this region prior to the MJO phase 8 (not shown).

Overall, prior to the MJO phase 8, the mixed layer experiences warming in the western and central Indian Ocean and cooling over the MC. The net heat flux drives the large scale warming pattern over the Indo-Pacific warm pool. In the western Indian Ocean, the mean state ocean currents advect the MLT warming due to the net heat flux and produce regions of enhanced warming that may seed the initial development of convection here. The ocean

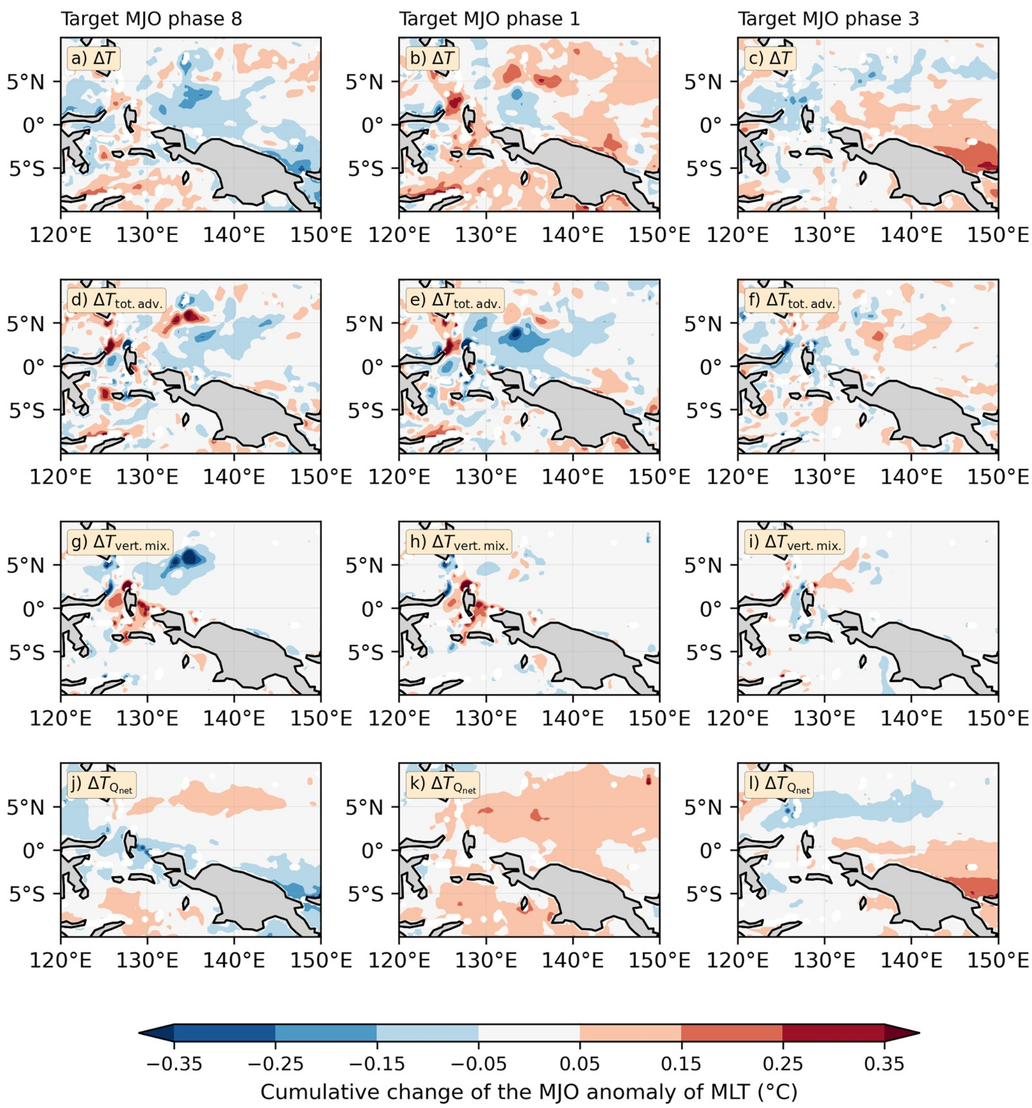

Figure 7. As Figure 3 but for the eastern Maritime Continent region.

advection contribution is weaker over the central Indian Ocean where the net heat flux dominates. Over the MC, the MJO-induced ocean current anomalies suppress the mean westward advection of warm MLT and thus contribute to cooling the MLT in this region, and promoting suppressed MJO convection over the MC.

3.2. MJO Phase 1: Initiation

MJO phase 1 represents the initiation stage of the MJO enhanced convective anomalies over the western Indian Ocean region. MJO phase 1 is often associated with the lowest forecast skill compared with other MJO phases (e.g., Karlowska et al., 2024a; Kim et al., 2014). In order to understand why models may predict MJO phase 1 with a worse skill, it is important to study the evolution of the SSTs during the growth of the MJO enhanced convective anomalies in the western Indian Ocean region prior to MJO phase 1.

Prior to MJO phase 1, the coupled model simulates suppressed MJO convection over the central Indian Ocean and the western MC at forecast day 1 in the forecast (Figure 2c). By forecast day 10, the canonical MJO phase 1 develops in the tropics, with enhanced MJO convective anomalies of −20 W m^{-2} over the western and central Indian Ocean and a suppressed MJO convective signal over the MC (Figure 2d). The coupled model reproduces the observed pattern well in this MJO phase (Figures 2i and 2j), albeit slightly underestimating the enhanced MJO convection over the central Indian Ocean region at forecast day 10 (Figures 2d and 2j).

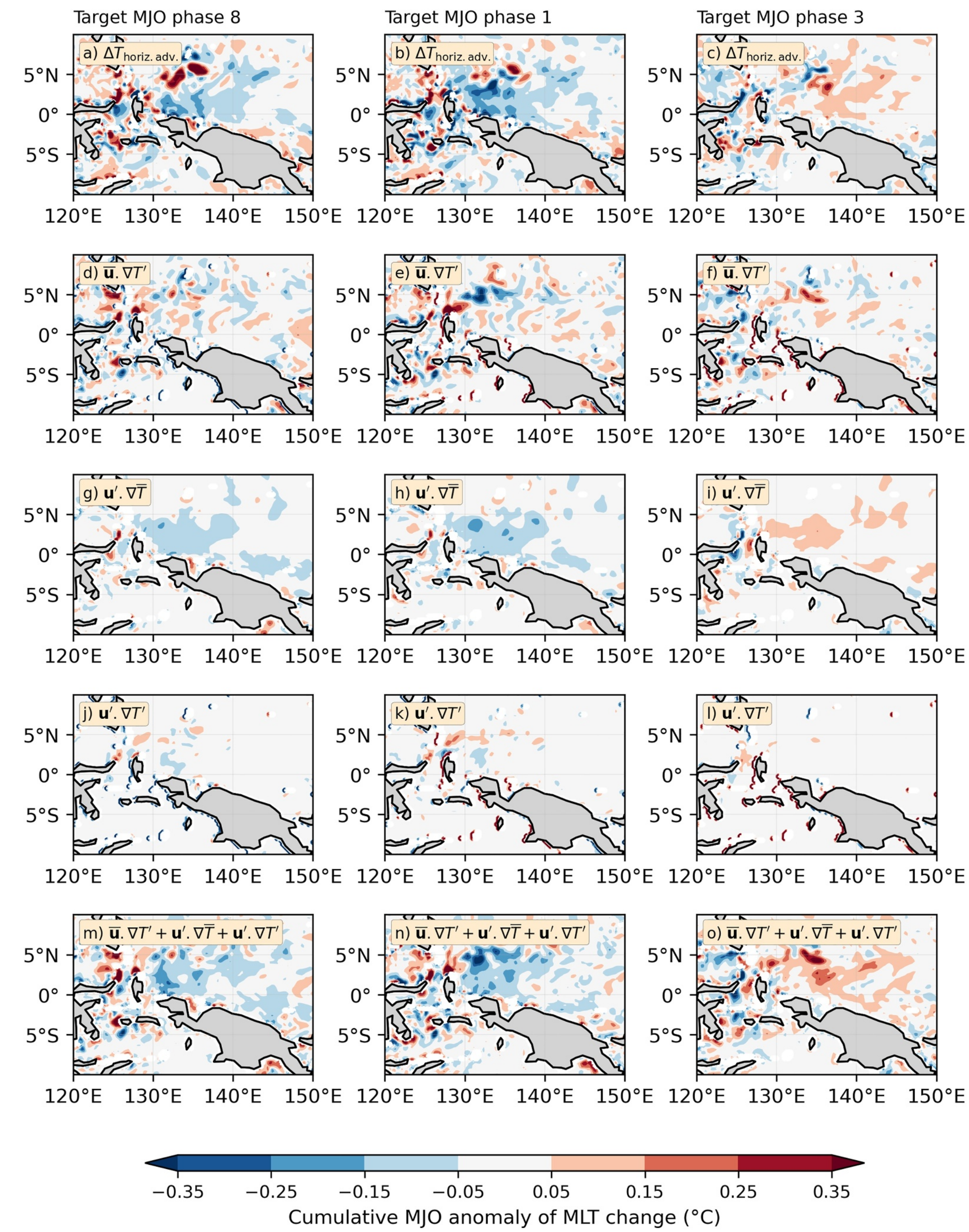

Figure 8. (a–c) Cumulative change in the MJO anomaly of mixed layer temperature (MLT) due to horizontal advection over forecast days 1–10 prior to the arrival of (target) MJO phases 8, 1, and 3; (d–f) advection of T' by $\overline{\mathbf{u}}$ over forecast days 1–10; (g–i) advection of $\overline{T}$ by u' over forecast days 1–10; (j–l) advection of T' by $\mathbf{u}'$ over forecast days 1–10; (m–o) sum of the advection of T' by $\overline{\mathbf{u}}$, the advection of $\overline{T}$ by u', and the advection of T' by $\mathbf{u}'$ over forecast days 1–10.

The development of the MJO convection over the Indian Ocean in the coupled model is preceded by warm MJO anomalies of SST in this region at forecast day 1 (i.e., 10 days prior to phase 1; Figure 1c). The warm MJO anomaly of SST in this region intensifies by forecast day 10 (i.e., the middle of phase 1; Figure 1d). Over the MC, the negative SST anomalies at forecast day 1 contribute to the development of suppressed MJO convection by forecast day 10 (Figure 2d).

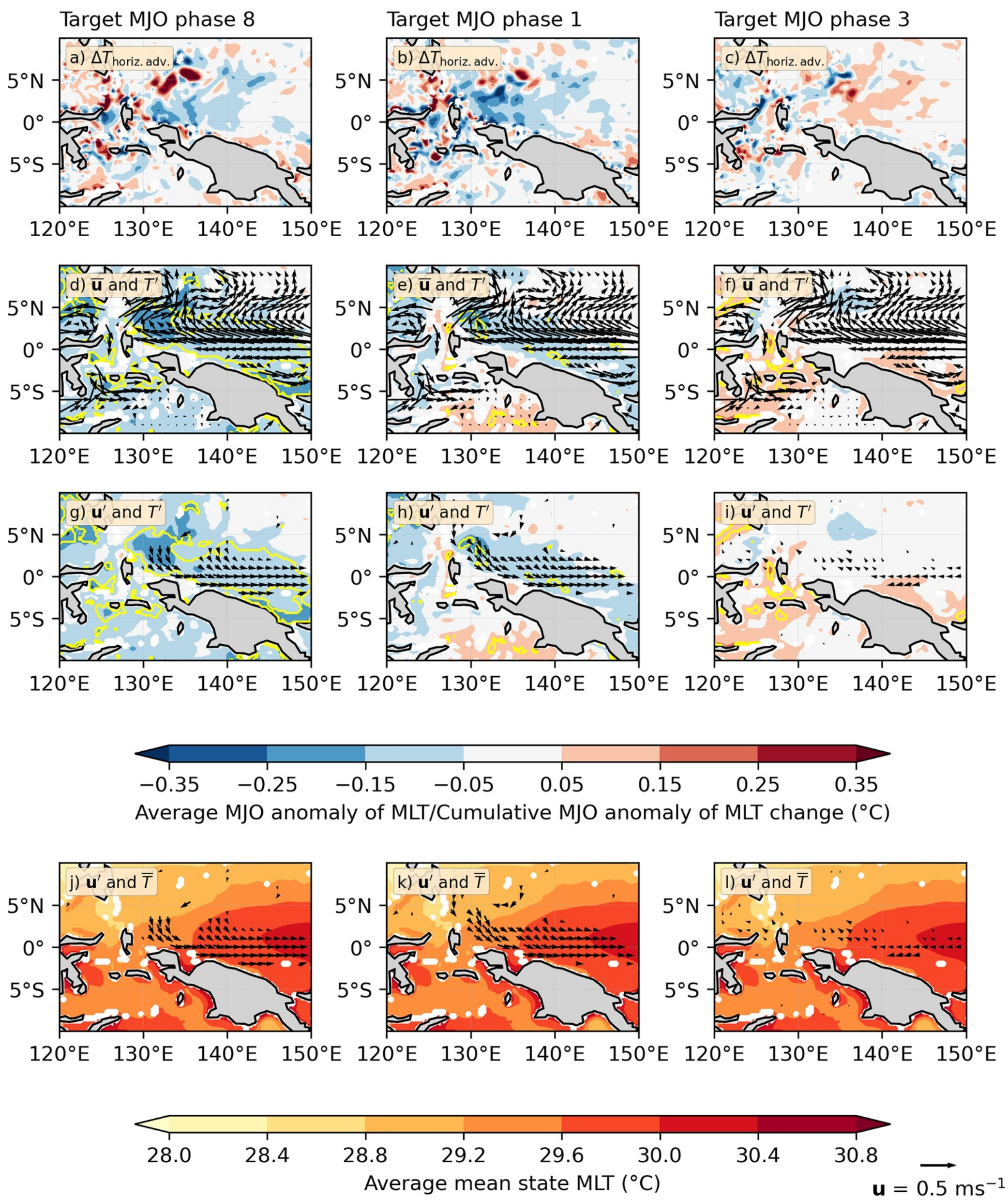

Figure 9. As in Figure 5 but for the eastern Maritime Continent region.

Similar to MJO phase 8, the development of the MJO convection over the Indian Ocean prior to MJO phase 1 is associated with a warming in the MJO anomaly of MLT in all three regions considered here (Figures 3b, 6b, and 7b). However, the strongest warming, of up to 0.5 °C, occurs in the western Indian Ocean (Figure 3b). This warming is especially strong close to the African coast. The central Indian Ocean region experiences a warming of up to 0.25 °C ahead of MJO phase 1 (Figure 6b). Over the eastern MC, the warming is less spatially coherent, and weaker than in the Indian Ocean, reaching a maximum of 0.15 °C (Figure 7b). The large scale warming pattern recorded across all regions considered prior to MJO phase 1 is contributed by the Q_{net} (Figures 3k, 6k, and 7k). All regions display a uniform warming due to the Q_{net} of up to 0.15 °C prior to MJO phase 1. This is in response to the large scale suppressed MJO conditions over the tropics at forecast day 1 (Figure 2c). This is also consistent with the shoaling of the MJO anomalies of the mixed layer in all three regions by up to 14 m (western Indian Ocean in Figure 4e, central Indian Ocean and eastern Maritime Continent regions in panels e in Figures S8 and S9 in Supporting Information S1, respectively).

Similar to target MJO phase 8, ocean advection is the second most important term driving the MJO anomalies of MLT prior to the start of MJO phase 1. Total advection produces strong positive MLT anomalies of up to 0.5 °C in the western Indian Ocean along the coast of Africa (Figure 3e). Horizontal advection dominates the total advection term in the western Indian Ocean prior to MJO phase 1 (Figure 5b). This MLT warming is likely driven by the mean state ocean currents advecting warm MJO anomalies of MLT toward and along the coast of Africa (Figure 5e). These warm MJO anomalies of MLT are significant at the 95% significance level (yellow outline in Figure 5h). The MJO-induced anomalous ocean currents are noisy and dominated by eddy-like circulations (not shown); the relatively short (5-year) data set is not sufficiently long to robustly determine if these anomalous currents consistently contribute to the advection term here.

A strong negative MJO anomaly of MLT is recorded in the coupled model at the equator between 60 °E and 70 °E prior to the MJO phase 1 (Figures 3b and 6b). This decrease of 0.25 °C in MLT is driven by ocean advection (Figures 3e and 6e). This is consistent with the development of the SST anomalies in these regions prior to MJO phase 1 (Figures 1c and 1d). Warm SST anomalies of up to 0.25 °C at forecast day 1 are advected west from the central Indian Ocean region toward the African coast. These anomalies are replaced in the central Indian Ocean region by relatively colder SST anomalies (<0.05 °C, white shading in Figures 1c and 1d) that are advected from further east.

The ocean advection tendency reinforces Q_{net} along the African coast (Figures 3e and 3k); however, over the eastern MC, advective MLT cooling (Figure 7e) opposes warming due to Q_{net} anomalies (Figure 7k). There is strong advective cooling of MLT located near the Halmahera eddy, north of the equator at around 130 °E. MJO wind anomalies induce southeastward ocean current anomalies that weaken the South Equatorial Current off the coast of New Guinea. These anomalous currents are directed up the mean gradient in MLT (Figure 9k), thus producing anomalous cooling there (Figure 8h). The other terms, $\overline{\mathbf{u}}.\nabla T'$ and $\mathbf{u}'.\nabla T'$, do not produce a spatially coherent pattern of cooling in this region prior to the MJO phase 1 (Figures 8e and 8k).

The vertical mixing contributions to the changes in the MJO anomaly of MLT prior to the MJO phase 1 are negligible in the central Indian Ocean region (Figure 6h) and the eastern MC (Figure 7h). The only region where the vertical mixing takes a larger role prior to MJO phase 1 is the western Indian Ocean region. The vertical mixing tendency of up to 0.25 °C locally reinforces the contributions of ocean advection and Q_{net} near the African coast (Figure 3h). Vertical mixing opposes the ocean advection at the location of the Great Whirl off the coast of Somalia at 8 °N, 55 °E (see mean state ocean currents in Figure 5e). This is consistent with the shoaling of the MJO anomaly of D20 in this region (Figure 4b) that will promote the entrainment of colder water by increasing the vertical temperature gradient below the mixed layer.

Overall, prior to the MJO phase 1, net heat flux is the dominant driver of the large scale warming in the Indo-Pacific warm pool. Horizontal advection of MLT anomalies reinforces the net heat flux warming near the African coast prior to the MJO phase 1. Over the MC, the MJO-induced ocean current anomalies produce MLT cooling, opposing the large scale warming tendency associated with the net heat flux in this region.

3.3. MJO Phase 3: Maturity

MJO phase 3 represents the maturity stage of the MJO enhanced convective anomalies over the western Indian Ocean region. This phase was chosen to study processes that drive the evolution of the SSTs once the MJO enhanced convective anomalies are established over the western Indian Ocean, and when these anomalies travel eastward into the central Indian Ocean and start to develop over the Maritime Continent in MJO phase 3.

Ten days prior to MJO phase 3, there is a weak enhanced MJO convection over the western and central Indian Ocean and a suppressed MJO convection over the MC in the coupled model (Figure 2e). By forecast day 10, MJO phase 3 arrives with a strong MJO convective anomaly over the whole tropical Indian Ocean and most of the MC (Figure 2f). The observations show a similar evolution of the MJO convective anomalies prior to MJO phase 3 (Figures 2k and 2l), albeit with a less elongated pattern of enhanced MJO convection over the Indian Ocean at forecast day 10.

The development of the MJO convective anomalies over the Indian Ocean is preceded by warm MJO SST anomalies of 0.25 °C in the central Indian Ocean at forecast day 1 (Figure 1e). These warm SST anomalies weaken over the Indian Ocean due to the intensification of the MJO convection that enhances cloud cover and increases mechanical mixing due to stronger surface winds (Figures 1f and 2f).

The change in the MJO anomaly of MLT over 10 days prior to the arrival of the MJO phase 3 is negative over the western Indian Ocean (Figure 3c). The cold MLT anomalies of up to −0.35 °C are centered around the equator in this region and are driven by the total advection (Figure 3f) and vertical mixing terms (Figure 3i), with a negligible contribution from Q_{net} (Figure 3l). There is a negative MJO anomaly of MLT located at the equator in the western Indian Ocean prior to MJO phase 3 (Figure 5f). It is likely that the mean state ocean currents advect this cool MLT anomaly westwards toward the African coast, contributing to the cooling west of 50°E. There is a small (approximately 3° × 1.75°) region of statistically significant current anomalies at the equator near the African coast, which would advect the colder mean state MLT off the coast of Africa toward the east, thus contributing to this negative MLT tendency (Figure 5l). However, it is unclear what causes the cooling tendency around 55°E, which may be driven by statistically insignificant eddy-driven heat fluxes. There are no coherent changes in the MJO anomaly of D20 prior to MJO phase 3 in this region (Figure 4c). The MJO anomaly of mixed layer depth shows a deepening of up to 6 m south of the equator in this region (Figure 4f), but this does not appear to contribute to the cooling tendency from vertical mixing along the equator (Figure 3i).

The MJO anomaly of MLT in the central Indian Ocean region and the eastern MC is mostly driven by Q_{net} prior to MJO phase 3 (Figures 6c, 6l, 7c, and 7l). The central Indian Ocean experiences an MLT cooling of up to −0.15 °C prior to MJO phase 3, consistent with the development of MJO convection in this region from forecast day 1–10. The eastern MC region displays a warming in MLT near New Guinea, and cooling in the Sulawesi sea. The warming due to Q_{net} is consistent with the shoaling of the mixed layer in this region prior to MJO phase 3 by up to 14 m (panel f in Figure S9 in Supplementary Information S1). Warm advection produces up to 0.15 °C of warming north of New Guinea, near the location of the Halmahera eddy (Figure 7f). The Reynolds decomposition suggests that this warming is due to the MJO anomalous ocean currents strengthening the mean state currents that advect relatively warm mean state MLT from the equator northwards toward the Philippines (Figures 8i and 9l). The other terms, $\bar{\mathbf{u}}.\nabla T'$ and $\mathbf{u}'.\nabla T'$, do not produce a spatially coherent pattern of warming in this region prior to the MJO phase 3 (Figures 8f and 8l). The vertical mixing contributions to the changes in the MJO anomaly of MLT prior to MJO phase 3 are negligible in the central Indian Ocean region (Figure 6i) and the eastern MC (Figure 7i). The total advection term in the central Indian Ocean region is noisy prior to MJO phase 3 and no coherent features can be inferred (Figure 6f).

Overall, prior to the MJO convection over the central Indian Ocean in phase 3, the MJO-induced MLT tendency is dominated by ocean advection and vertical mixing in the western Indian Ocean and by net heat flux in the central Indian Ocean and over the MC.

3.4. The Importance of Different Horizontal Scales in the Mixed Layer Heat Budget on the MJO Timescales

The coupled model shows that Q_{net} dominates the large-scale changes in the MJO anomalies of MLT. However, ocean advection and vertical mixing can substantially modulate the total MJO anomaly of MLT, reinforcing or opposing the changes due to Q_{net}. To determine the relative importance of these oceanic processes in the MJO mixed layer heat budget across a range of spatial scales, a Gaussian smoothing was applied to the two-dimensional MLT tendency anomaly fields for a selection of smoothing radii (1°, 2°, 4°, 8°, 16°, 32°). The covariance was then calculated between each budget term and the total MLT change (Figure 10).

Prior to MJO phase 8, the ocean advection is the dominant term at smoothing radii smaller than 4° across all regions considered here (Figures 10a, 10d, and 10g). At larger horizontal scales, Q_{net} displays the largest covariance in the western Indian Ocean region and over the eastern MC. In the central Indian Ocean, ocean advection and Q_{net} show a similar covariance to the total MLT change at larger horizontal scales.

Prior to MJO phase 1, the transition in dominance between ocean advection and Q_{net} happens at a larger horizontal scale in the Indian Ocean compared with target MJO phase 8, closer to 16° (Figures 10b and 10e). This change could be associated with large-scale equatorial oceanic Kelvin and Rossby waves that advect MJO anomalies of MLT across the Indian Ocean. However, the signal is not robust enough in the ocean current anomalies in this coupled model. The covariance of the advection term in target MJO phase 1 is approximately three times stronger than the covariance of the Q_{net} term (Figures 10b, 10e, and 10h). In contrast, in target MJO phase 8, the covariance of the advection term is only slightly larger than the Q_{net} covariance, thus the transition in dominance between ocean advection and Q_{net} is at a smaller horizontal scale in target MJO phase 1 than in target MJO phase 8.

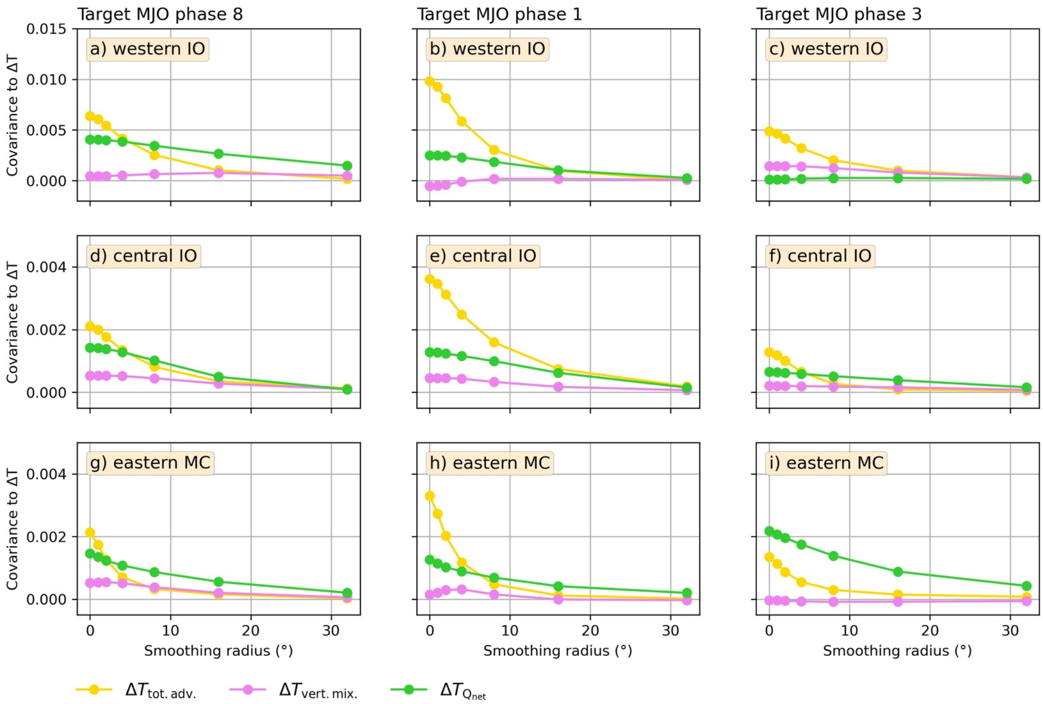

Figure 10. Covariance between the cumulative change in the MJO anomaly of mixed layer temperature, and each temperature tendency term, as a function of the smoothing radius. The temperature tendency terms are $\Delta T_{\mathrm{tot.\ adv.}}$ (yellow), $\Delta T_{\mathrm{vert.\ mix.}}$ (pink), and $\Delta T_{Q_{net}}$ (green). The covariances are calculated over forecast days 1–10 prior to the arrival of target MJO phases 8 (left column), 1 (central column) and 3 (right column), for the western Indian Ocean (IO) region (panels a–c), central IO region (panels d–f) and eastern Maritime Continent region (panels g–i).

Prior to MJO phase 3, each region displays a more complex interplay between the three processes than in phase 8 or 1. In the western Indian Ocean region, ocean advection is dominant at all horizontal scales, with vertical mixing displaying the second largest covariance and Q_{net} being negligible at all horizontal scales (Figure 10c). In the central Indian Ocean, ocean advection dominates at smaller horizontal scales (<4°) and Q_{net} has the largest covariance at horizontal scales >4° (Figure 10f). Finally, in the eastern MC, Q_{net} dominates at all horizontal scales prior to MJO phase 3, with advection having a secondary contribution to the changes in the MJO anomaly of MLT there (Figure 10i).

4. Discussion and Conclusions

The mixed layer heat budget of the coupled ocean–atmosphere Numerical Weather Prediction model of the UK Met Office reveals that ocean advection plays an important role in modulating intraseasonal mixed layer temperature (MLT) anomalies in the Indo-Pacific warm pool region. The coupled model shows that net heat fluxes drive the large-scale (order 10°) changes to the intraseasonal MLT anomalies, but ocean advection dominates at smaller horizontal scales (order 1°) and contributes significant changes to these MLT anomalies.

Prior to the MJO initiation over the western Indian Ocean (RMM phase 1), the mixed layer shoals and the net surface heat fluxes (distributed over a shallower mixed layer) lead to an overall warming over the Indo-Pacific warm pool. The advection of the intraseasonal MLT anomalies by the mean state ocean currents in the western Indian Ocean reinforces the warming in this region due to the net surface heat flux. Over the Maritime Continent, the MJO-induced ocean current anomalies oppose the mean state ocean currents (and mesoscale eddy circulation) to resulting in anomalous cooling from the reduced advection of warm mean state MLT from the east, thus reducing the warming due to the net heat flux in this region.

When the MJO convection is developing over the central Indian Ocean (RMM phase 3), the situation is more complex. The western Indian Ocean experiences cooling after the MJO passage. This cooling is likely associated with the mean state ocean currents advecting cold MJO anomaly of MLT toward the coast of Africa. In the central

Indian Ocean region, the cooling due to the development of the MJO convective phase is driven by the net heat fluxes only. Over the eastern Maritime Continent, the net heat fluxes are driving most of the total MLT changes on MJO timescales. However, there is a small and positive contribution in this region from the MJO-induced ocean current anomalies that strengthen the mean currents in this region.

RMM phases 8, 1, and 3 were investigated in this study to represent different stages of the evolution of the MJO-enhanced convective anomalies in the western Indian Ocean region. The mixed layer heat budget was conducted for all RMM phases and the results are as follows. The intraseasonal mixed layer heat budget in the western Indian Ocean region is dominated by ocean advection at small scales across all target MJO phases (Figures S1–S2 in Supporting Information S1). In this region, the net heat flux contributes to the large-scale warming (cooling) of the intraseasonal MLT anomaly prior to MJO phases 8 to 2 (6–7) (Figures S1–S2 in Supporting Information S1). Prior to MJO phases 6 and 7, the net heat flux cooling occurs off the equator, whereas prior to MJO phases 8 to 2 the warming pattern occurs both at the equator and off the equator. The net heat flux is not important in this region prior to MJO phases 3 to 5. The net heat flux is the dominant driver of the intraseasonal MLT changes in the central Indian Ocean region across all target MJO phases (Figures S3–S4 in Supporting Information S1). In the eastern MC, the cooling due to ocean advection in the area of the Halmahera eddy occurs only prior to MJO phases 7 to 2 (Figures S5–S6 in Supporting Information S1). The net heat flux, however, drives the large scale warming and cooling patterns in this region across all target MJO phases.

The MJO mixed layer heat budget we have conducted using the coupled NWP model of the UK Met Office is broadly consistent with the ocean state estimate mixed layer heat budget of Halkides et al. (2015). Halkides et al. (2015) demonstrated that the net heat fluxes are the most dominant off the equator during the MJO, while the horizontal advection is the biggest driver of the intraseasonal MLT changes at the equator during the MJO. Our results broadly corroborate the results of Halkides et al. (2015); however, the horizontal advection contribution in some places in this study extends some distance away from the equator (western Indian Ocean region; Figures 5a–5c), while in others, no dominant signal is found in the advective term (central Indian Ocean region; Figures 6d–6f). Our forecast model suggests that both the ocean advection and the net heat fluxes are important, but they act on different horizontal scales to modulate the intraseasonal changes in the MLT. The net heat flux dominates at larger horizontal scales (order 10°), while ocean advection dominates at smaller horizontal scales (order 1°). An in situ mixed layer heat budget of Vijith et al. (2020) corroborates our findings, showing that ocean advection has a significant contribution to the mixed layer heat budget at small horizontal scales north of the central Indian Ocean region, in Bay of Bengal. The boreal summer intraseasonal oscillation (BSISO) that propagates northwards over the Bay of Bengal is one of the triggering mechanism for the onset of the Asian summer monsoon (K. Li et al., 2013). Akin to the MJO, the BSISO can modulate the wind stress and the heat flux at the ocean surface, affecting the mixed layer depth and the MLT over the Bay of Bengal (Jia et al., 2023). A potential future study should extend our analysis of the coupled NWP model of the UK Met Office to the Bay of Bengal to understand different processes governing the evolution of the MLT in this forecast model during the northward propagation of the BSISO.

The westerly wind bursts associated with the MJO increase the cyclonic eddy generation in the Banda Sea during boreal winter season (Hao et al., 2023). The coupled model of the UK Met Office shows important contributions from the ocean advection in the Halmahera eddy region to the MJO anomalies of MLT over the eastern Maritime Continent region. The MJO-induced ocean currents in the model lead to a cyclonic circulation in phases 1 and 8 in this region. The Halmahera eddy is known to be weaker during boreal winter (Ramadhan et al., 2020); therefore, our results pose the question of whether the MJO reduces the anti-cyclonic circulation in this region, and whether the MJO affects the vertical heat transfer from below the mixed layer toward the surface within the area of this eddy.

The MJO is also reported to modulate the strength of the Indonesian Throughflow, which in turn regulates the exchange of water between the eastern Indian Ocean basin and the western tropical Pacific Ocean basin (Gordon et al., 2019; Tamasiunas et al., 2021). Tamasiunas et al. (2021) shown that 50% of the Indonesian Throughflow transport is regulated by the MJO, and the convective (suppressed) phase of the MJO leads to a reduction (enhancement) of the Indonesian Throughflow transport. Our forecast model suggests that the MJO does modulate ocean currents in the Indonesian Throughflow area, raising implications for the heat and water transport between these ocean basins in models that do not resolve the interaction between the MJO and the mesoscale eddy circulations in this region. Additionally, vertical mixing is found to contribute a substantial cooling near the area of the Great Whirl off the coast of Africa prior to the MJO phases 8 and 1 in this coupled model. The thermocline shoals in this region prior to the MJO phases 8 and 1, and consistently, the model records entrainment of cooler water from below the mixed layer there. Computer resources already allow for global models to use eddy-resolving ocean resolutions (Roberts et al., 2016). Therefore, the interactions between the mesoscale eddies and the MJO should be investigated further in future studies.

In conclusion, the mixed layer heat budget of the coupled model of the UK Met Office reveals important contributions from the subsurface ocean processes to the intraseasonal MLT anomalies in the Indo-Pacific warm pool region. Ocean advection drives the small scale changes in the intraseasonal MLT anomalies, while the net heat flux provides large scale warming and cooling patterns. Overall, ocean advection should be well-simulated to accurately forecast the MJO.

Data Availability Statement

Daily interpolated OLR values were obtained from National Oceanic and Atmospheric Administration (Liebmann & Smith, 1996) available at https://psl.noaa.gov/data/gridded/data.olrcdr.interp.html. Observed RMM indices (Wheeler & Hendon, 2004) were retrieved from Bureau of Meteorology, available at http://www.bom.gov.au/climate/mjo/. Figures were made with Matplotlib version 3.3.4 (Caswell et al., 2021; Hunter, 2007). Data to generate the figures can be accessed at https://www.zotero.org/e.karlowska/collections/WJJ6IRGP.

Acknowledgments

EK was supported by the Natural Environment Research Council and ARIES DTP (Grant number NE/S007334/1). AJM was partially funded by the Natural Environment Research Council TerraMaris project (Grant NE/R016704/1).

References

Blockley, E. W., Martin, M. J., McLaren, A. J., Ryan, A. G., Waters, J., Lea, D. J., et al. (2014). Recent development of the Met Office operational ocean forecasting system: An overview and assessment of the new Global FOAM forecasts. *Copernicus GmbH*, *7*(6), 2613–2638. https://doi.org/10.5194/gmd-7-2613-2014

Caswell, T. A., Droettboom, M., Lee, A., de Andrade, E. S., Hunter, J., Firing, E., et al. (2021). matplotlib/matplotlib: REL: V3.3.4 [Software]. *Zenodo*. https://doi.org/10.5281/zenodo.4475376

Chandra, A., Keenlyside, N., Svendsen, L., & Singh, A. (2024). Processes driving subseasonal variations of upper ocean heat content in the equatorial Indian Ocean. *Journal of Geophysical Research: Oceans*, *129*(2), e2023JC020074. https://doi.org/10.1029/2023JC020074

Chi, N. H., Lien, R. C., D'Asaro, E. A., & Ma, B. B. (2014). The surface mixed layer heat budget from mooring observations in the central Indian Ocean during Madden–Julian Oscillation events. *Journal of Geophysical Research: Oceans*, *119*(7), 4638–4652. https://doi.org/10.1002/2014JC010192

de Boyer Montégut, C., Madec, G., Fischer, A. S., Lazar, A., & Iudicone, D. (2004). Mixed layer depth over the global ocean: An examination of profile data and a profile-based climatology. *Journal of Geophysical Research*, *109*(C12), 1–20. https://doi.org/10.1029/2004JC002378

de Boyer Montégut, C., Mignot, J., Lazar, A., & Cravatte, S. (2007). Control of salinity on the mixed layer depth in the world ocean: 1. General description. *Journal of Geophysical Research*, *112*(C6), C06011. https://doi.org/10.1029/2006JC003953

DeMott, C. A., Klingaman, N. P., & Woolnough, S. J. (2015). Atmosphere-ocean coupled processes in the Madden-Julian oscillation. *Blackwell Publishing Ltd*, *53*(4), 1099–1154. https://doi.org/10.1002/2014RG000478

Donlon, C. J., Martin, M., Stark, J., Roberts-Jones, J., Fiedler, E., & Wimmer, W. (2012). The operational Sea Surface temperature and sea ice analysis (OSTIA) system. *Remote Sensing of Environment*, *116*, 140–158. https://doi.org/10.1016/j.rse.2010.10.017

Drushka, K., Sprintall, J., & Gille, S. T. (2014). Subseasonal variations in salinity and barrier-layer thickness in the eastern equatorial Indian Ocean. *Journal of Geophysical Research: Oceans*, *119*(2), 805–823. https://doi.org/10.1002/2013JC009422

Drushka, K., Sprintall, J., Gille, S. T., & Wijffels, S. (2012). In situ observations of Madden–Julian Oscillation mixed layer dynamics in the Indian and western Pacific Oceans. *Journal of Climate*, *25*(7), 2306–2328. https://doi.org/10.1175/JCLI-D-11-00203.1

Duchon, C. E. (1979). Lanczos filtering in one and two dimensions. *Journal of Applied Meteorology and Climatology*, *18*(8), 1016–1022. https://doi.org/10.1175/1520-0450(1979)018<1016:lfioat>2.0.co;2

Fiedler, E. K., Mao, C., Good, S. A., Waters, J., & Martin, M. J. (2019). Improvements to feature resolution in the OSTIA sea surface temperature analysis using the NEMOVAR assimilation scheme. *Quarterly Journal of the Royal Meteorological Society*, *145*(725), 3609–3625. https://doi.org/10.1002/qj.3644

Fiedler, P. C. (2010). Comparison of objective descriptions of the thermocline. *Limnology and Oceanography: Methods*, *8*(6), 313–325. https://doi.org/10.4319/lom.2010.8.313

Good, S., Fiedler, E., Mao, C., Martin, M. J., Maycock, A., Reid, R., et al. (2020). The current configuration of the OSTIA system for operational production of foundation sea surface temperature and ice concentration analyses. *Remote Sensing*, *12*(4), 720. https://doi.org/10.3390/rs12040720

Gordon, A. L., Napitu, A., Huber, B. A., Gruenburg, L. K., Pujiana, K., Agustiadi, T., et al. (2019). Makassar Strait throughflow seasonal and interannual variability: An overview. *Journal of Geophysical Research: Oceans*, *124*(6), 3724–3736. https://doi.org/10.1029/2018jc014502

Gottschalck, J., Wheeler, M., Weickmann, K., Vitart, F., Savage, N., Lin, H., et al. (2010). A framework for assessing operational Madden-Julian oscillation forecasts: A clivar MJO working group project. *Bulletin of the American Meteorological Society*, *91*(9), 1247–1258. https://doi.org/10.1175/2010BAMS2816.1

Gregory, D., & Allen, S. (1991). The effect of convective downdraughts upon NWP and climate simulations. In (pp. 122–123).

Gregory, D., & Rowntree, P. R. (1990). A mass flux convection scheme with representation of cloud ensemble characteristics and stability-dependent closure. *Monthly Weather Review*, *118*(7), 1483–1506. https://doi.org/10.1175/1520-0493(1990)118⟨1483:AMFCSW⟩2.0.CO;2

Halkides, D. J., Waliser, D. E., Lee, T., Menemenlis, D., & Guan, B. (2015). Quantifying the processes controlling intraseasonal mixed-layer temperature variability in the tropical Indian Ocean. *Journal of Geophysical Research: Oceans*, *120*(2), 692–715. https://doi.org/10.1002/2014JC010139

Hao, Z., Xu, Z., Feng, M., Zhang, P., You, J., & Yin, B. (2023). Seasonal variability of eddy kinetic energy in the Banda Sea revealed by an ocean model: An energy budget perspective. *Deep Sea Research Part II: Topical Studies in Oceanography*, *211*, 105320. https://doi.org/10.1016/J.DSR2.2023.105320

Hendon, H. H., & Glick, J. (1997). Intraseasonal air–sea interaction in the tropical Indian and Pacific Oceans. *Journal of Climate*, *10*(4), 647–661. https://doi.org/10.1175/1520-0442(1997)010⟨0647:IASIIT⟩2.0.CO;2

Hosoda, S., Ohira, T., Sato, K., & Suga, T. (2010). Improved description of global mixed-layer depth using Argo profiling floats. *Journal of Oceanography*, *66*(6), 773–787. https://doi.org/10.1007/s10872-010-0063-3

Hunter, J. D. (2007). Matplotlib: A 2D graphics environment. *Computing in Science & Engineering*, *9*(3), 90–95. https://doi.org/10.1109/MCSE.2007.55

Itterly, K., Taylor, P., & Roberts, J. B. (2021). Satellite perspectives of Sea Surface temperature diurnal warming on atmospheric moistening and radiative heating during MJO. *Journal of Climate*, *34*(3), 1203–1226. https://doi.org/10.1175/JCLI-D-20-0350.1

Jia, W., Sun, J., Zhang, W., & Wang, H. (2023). The effect of boreal summer intraseasonal oscillation on mixed layer and upper ocean temperature over the South China Sea. *Journal of Ocean University of China*, *22*(2), 285–296. https://doi.org/10.1007/s11802-023-5008-8

Karlowska, E., Matthews, A. J., Webber, B. G. M., Graham, T., & Xavier, P. (2024a). The effect of diurnal warming of sea-surface temperatures on the propagation speed of the Madden–Julian oscillation. *Quarterly Journal of the Royal Meteorological Society*, *150*(758), 334–354. https://doi.org/10.1002/qj.4599

Karlowska, E., Matthews, A. J., Webber, B. G. M., Graham, T., & Xavier, P. (2024b). Two-way feedback between the Madden–Julian Oscillation and diurnal warm layers in a coupled ocean-atmosphere model. *Quarterly Journal of the Royal Meteorological Society, in Press*. https://doi.org/10.1002/qj.4807

Kim, H. M., Webster, P. J., Toma, V. E., & Kim, D. (2014). Predictability and prediction skill of the MJO in two operational forecasting systems. *Journal of Climate*, *27*(14), 5364–5378. https://doi.org/10.1175/JCLI-D-13-00480.1

Li, K., Yu, W., Li, T., Murty, V. S. N., Khokiattiwong, S., Adi, T. R., & Budi, S. (2013a). Structures and mechanisms of the first-branch northward-propagating intraseasonal oscillation over the tropical Indian Ocean. *Climate Dynamics*, *40*(7), 1707–1720. https://doi.org/10.1007/s00382-012-1492-z

Li, Y., Han, W., Shinoda, T., Wang, C., Lien, R.-C., Moum, J. N., & Wang, J.-W. (2013b). Effects of the diurnal cycle in solar radiation on the tropical Indian Ocean mixed layer variability during wintertime Madden-Julian Oscillations. *Journal of Geophysical Research: Oceans*, *118*(10), 4945–4964. https://doi.org/10.1002/JGRC.20395

Liebmann, B., & Smith, C. A. (1996). Description of a complete (interpolated) outgoing longwave radiation dataset [Dataset]. *Bulletin of the American Meteorological Society*, *77*(6), 1275–1277. Retrieved from https://psl.noaa.gov/data/gridded/data.olrcdr.interp.html

Liu, L., Li, Y., & Wang, F. (2021). MJO-induced intraseasonal mixed layer depth variability in the equatorial Indian Ocean and impacts on subsurface water obduction. *Journal of Physical Oceanography*, *51*(4), 1247–1263. https://doi.org/10.1175/JPO-D-20-0179.1

Madden, R. A., & Julian, P. R. (1971). Detection of a 40–50 day oscillation in the zonal wind in the tropical Pacific. *Journal of the Atmospheric Sciences*, *28*(5), 702–708. https://doi.org/10.1175/1520-0469(1971)028<0702:doadoi>2.0.co;2

Madden, R. A., & Julian, P. R. (1972). Description of global-scale circulation cells in the tropics with a 40–50 day period. *Journal of the Atmospheric Sciences*, *29*(6), 1109–1123. https://doi.org/10.1175/1520-0469(1972)029<1109:dogscc>2.0.co;2

Madec, G., Bourdallé-Badie, R., Bouttier, P.-A., Bricaud, C., Bruciaferri, D., Calvert, D., et al. (2017). NEMO ocean engine.

Madec, G., Delecluse, P., Imbard, M., & Levy, C. (1997). Ocean general circulation model reference manual. *Note du Pôle de modélisation*.

Matthews, A. J. (2000). Propagation mechanisms for the Madden-Julian Oscillation. *Quarterly Journal of the Royal Meteorological Society*, *126*(569), 2637–2651. https://doi.org/10.1002/qj.49712656902

Matthews, A. J. (2008). Primary and successive events in the Madden–Julian Oscillation. *Quarterly Journal of the Royal Meteorological Society*, *134*(631), 439–453. https://doi.org/10.1002/qj.224

McDougall, T. J., & Barker, P. M. (2011). Getting started with TEOS-10 and the Gibbs Seawater (GSW) oceanographic toolbox. *Scor/Iapso WG*, *127*(532), 1–28.

McPhaden, M. J., & Foltz, G. R. (2013). Intraseasonal variations in the surface layer heat balance of the central equatorial Indian Ocean: The importance of zonal advection and vertical mixing. *Geophysical Research Letters*, *40*(11), 2737–2741. https://doi.org/10.1002/GRL.50536

Megann, A. P., Storkey, D., Aksenov, Y., Alderson, S., Calvert, D., Graham, T., et al. (2014). Go 5.0: The joint NERC-Met office NEMO global ocean model for use in coupled and forced applications. *Geotechnical Model Development*, *7*(3), 1069–1092. https://doi.org/10.5194/gmd-7-1069-2014

Meyers, G. (1979). Annual variation in the slope of the 14°c isotherm along the equator in the Pacific Ocean. *Journal of Physical Oceanography*, *9*(5), 885–891. https://doi.org/10.1175/1520-0485(1979)009<0885:avitso>2.0.co;2

Paulson, C. A., & Simpson, J. J. (1977). Irradiance measurements in the upper ocean. *Journal of Physical Oceanography*, *7*(6), 952–956. https://doi.org/10.1175/1520-0485(1977)007<0952:imituo>2.0.co;2

Rae, J. G., Hewitt, H. T., Keen, A. B., Ridley, J. K., West, A. E., Harris, C. M., et al. (2015). Development of the global sea ice 6.0 CICE configuration for the met office global coupled model. *Geoscientific Model Development*, *8*(7), 2221–2230. https://doi.org/10.5194/gmd-8-2221-2015

Ramadhan, M. F., Sugianto, D. N., Wirasatriya, A., Setiyono, H., & Maslukah, L., & others. (2020). Characteristics of Halmahera Eddy and its relation to sea surface temperature, chlorophyll-a, and thermocline layer. *IOP Conference Series: Earth and Environmental Science*, *530*, 12039.

Rawlins, F., Ballard, S. P., Bovis, K. J., Clayton, A. M., Li, D., Inverarity, G. W., et al. (2007). The met office global four-dimensional variational data assimilation scheme. *Quarterly Journal of the Royal Meteorological Society*, *133*(623), 347–362. https://doi.org/10.1002/qj.32

Ridley, J. K., Blockley, E. W., Keen, A. B., Rae, J. G., West, A. E., & Schroeder, D. (2018). The sea ice model component of HadGEM3-GC3.1. *Geoscientific Model Development*, *11*(2), 713–723. https://doi.org/10.5194/gmd-11-713-2018

Roberts, M. J., Hewitt, H. T., Hyder, P., Ferreira, D., Josey, S. A., Mizielinski, M., & Shelly, A. (2016). Impact of ocean resolution on coupled air-sea fluxes and large-scale climate. *Geophysical Research Letters*, *43*(19), 10430–10438. https://doi.org/10.1002/2016GL070559

Rydbeck, A. V., Christophersen, J. A., Flatau, M. K., Janiga, M. A., Jensen, T. G., Reynolds, C. A., et al. (2023). Anchoring intraseasonal air–sea interactions: The moored moist static energy budget in the Indian ocean from reanalysis. *Journal of Climate*, *36*(3), 959–981. https://doi.org/10.1175/JCLI-D-22-0182.1

Rydbeck, A. V., Jensen, T. G., Smith, T. A., Flatau, M. K., Janiga, M. A., Reynolds, C. A., & Ridout, J. A. (2019). Ocean heat content and the intraseasonal oscillation. *Geophysical Research Letters*, *46*(24), 14558–14566. https://doi.org/10.1029/2019GL084974

Sobel, A. H., Maloney, E. D., Bellon, G., & Frierson, D. M. (2010). Surface fluxes and tropical intraseasonal variability: A reassessment. *Journal of Advances in Modeling Earth Systems*, *2*(1), 2. https://doi.org/10.3894/JAMES.2010.2.2

Storkey, D., Blaker, A. T., Mathiot, P., Megann, A., Aksenov, Y., Blockley, E. W., et al. (2018). UK global ocean GO6 and GO7: A traceable hierarchy of model resolutions. *Geoscientific Model Development*, *11*(8), 3187–3213. https://doi.org/10.5194/gmd-11-3187-2018

Tamasiunas, M. C. N., Shinoda, T., Susanto, R. D., Zamudio, L., & Metzger, E. J. (2021). Intraseasonal variability of the Indonesian throughflow associated with the Madden-Julian Oscillation. *Deep Sea Research Part II: Topical Studies in Oceanography*, *193*, 104985. https://doi.org/10.1016/j.dsr2.2021.104985

Vellinga, M., Copsey, D., Graham, T., Milton, S., & Johns, T. (2020). Evaluating benefits of two-way ocean–atmosphere coupling for global NWP forecasts. *Weather and Forecasting*, *35*(5), 2127–2144. https://doi.org/10.1175/WAF-D-20-0035.1

Vijith, V., Vinayachandran, P. N., Webber, B. G. M., Matthews, A. J., George, J. V., Kannaujia, V. K., et al. (2020). Closing the sea surface mixed layer temperature budget from in situ observations alone: Operation Advection during BoBBLE. *Scientific Reports*, *10*(1), 7062. https://doi.org/10.1038/s41598-020-63320-0

Walters, D., Baran, A. J., Boutle, I., Brooks, M., Earnshaw, P., Edwards, J., et al. (2019). The met office unified model global atmosphere 7.0/7.1 and JULES global land 7.0 configurations. *Geoscientific Model Development*, *12*(5), 1909–1963. https://doi.org/10.5194/gmd-12-1909-2019

Walters, D., Boutle, I., Brooks, M., Melvin, T., Stratton, R., Vosper, S., et al. (2017). The met office unified model global atmosphere 6.0/6.1 and JULES global land 6.0/6.1 configurations. *Geoscientific Model Development*, *10*(4), 1487–1520. https://doi.org/10.5194/gmd-10-1487-2017

Waters, J., Lea, D. J., Martin, M. J., Mirouze, I., Weaver, A., & While, J. (2015). Implementing a variational data assimilation system in an operational 1/4 degree global ocean model. *Quarterly Journal of the Royal Meteorological Society*, *141*(687), 333–349. https://doi.org/10.1002/qj.2388

Webber, B. G. M., Matthews, A. J., Heywood, K. J., & Stevens, D. P. (2012a). Ocean Rossby waves as a triggering mechanism for primary Madden–Julian events. *Quarterly Journal of the Royal Meteorological Society*, *138*(663), 514–527. https://doi.org/10.1002/qj.936

Webber, B. G. M., Stevens, D. P., Matthews, A. J., & Heywood, K. J. (2012b). Dynamical ocean forcing of the Madden-Julian oscillation at lead times of up to five months. *Journal of Climate*, *25*(8), 2824–2842. https://doi.org/10.1175/JCLI-D-11-00268.1

Wheeler, M. C., & Hendon, H. H. (2004). An all-season real-time multivariate MJO index: Development of an index for monitoring and prediction. *Monthly Weather Review*, *132*(8), 1917–1932. Retrieved from http://www.bom.gov.au/climate/mjo/#tabs=Monitoring

Woolnough, S. J., Slingo, J. M., & Hoskins, B. J. (2000). The relationship between convection and sea surface temperature on intraseasonal timescales. *Journal of Climate*, *13*(12), 2086–2104. https://doi.org/10.1175/1520-0442(2000)013⟨2086:TRBCAS⟩2.0.CO;2

Woolnough, S. J., Vitart, F., & Balmaseda, M. A. (2007). The role of the ocean in the Madden–Julian Oscillation: Implications for MJO prediction. *Quarterly Journal of the Royal Meteorological Society*, *133*(622), 117–128. https://doi.org/10.1002/qj.4

Yan, Y., Zhang, L., Yu, Y., Chen, C., Xi, J., & Chai, F. (2021). Rectification of the intraseasonal SST variability by the diurnal cycle of SST revealed by the global tropical moored Buoy Array. *Geophysical Research Letters*, *48*(1), e2020GL090913. https://doi.org/10.1029/2020GL090913

Zhang, C. (2005). Madden-Julian Oscillation. *Reviews of Geophysics*, *43*(2), RG2003. https://doi.org/10.1029/2004RG000158